Recent progress in weak lensing study

T. Futamase

Astronomical Institute,

Tohoku University, Sendai, Japan

10th Dec. 08 @KEK

- Introduction to weak lensing
- Weak lensing analysis of clusters of galaxies

  A1689

  T. Broadhurst(?), K.Umetsu(ASIAA), M.Takada(IPMU) and T.F

  Coma cluster

  N. Okabe(Tohoku) and T.F
- HOLICs and its application to A1689

  Y. Ookura (Tohoku) and T.F

What is gravitational lensing?

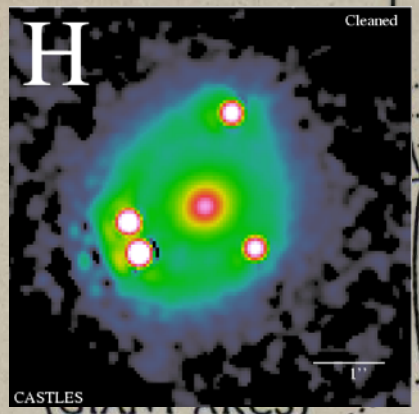

Lensing object

source

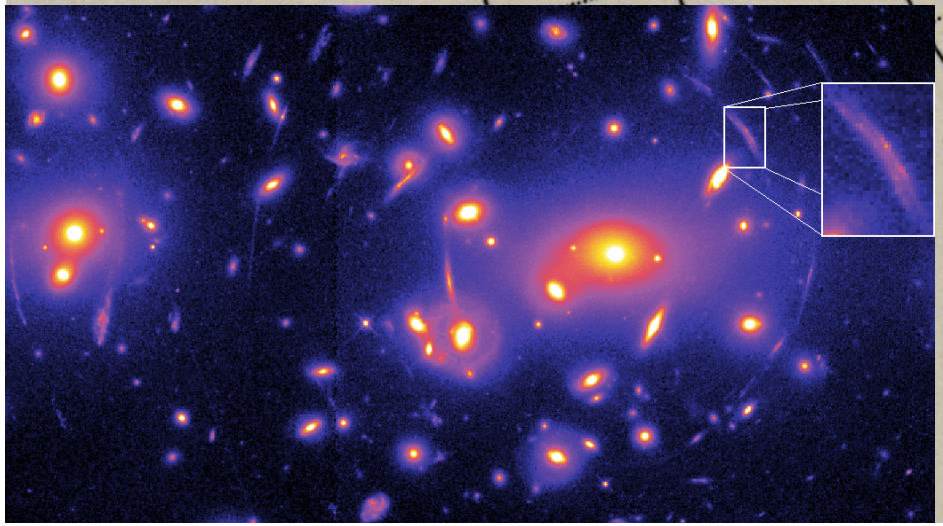

Why gravitational lensing?

(1) Gravitational lensing is a unique method to study masses of cosmic structures independent of <M/L>

- Depends only on **gravity** (based on the general relativity)
- No need of any assumption on "**dynamical state"** or "**matter content"** of the system
  baryonic matter <=> dark matter
- Complementary to other methods **(X-ray, SZ effect, optical**

(2) Importance as means of cosmological tests since it depends also on the global geometry of the universe

- Measurement of cosmological parameters
  Dark energy equation of state

Weak Lensing

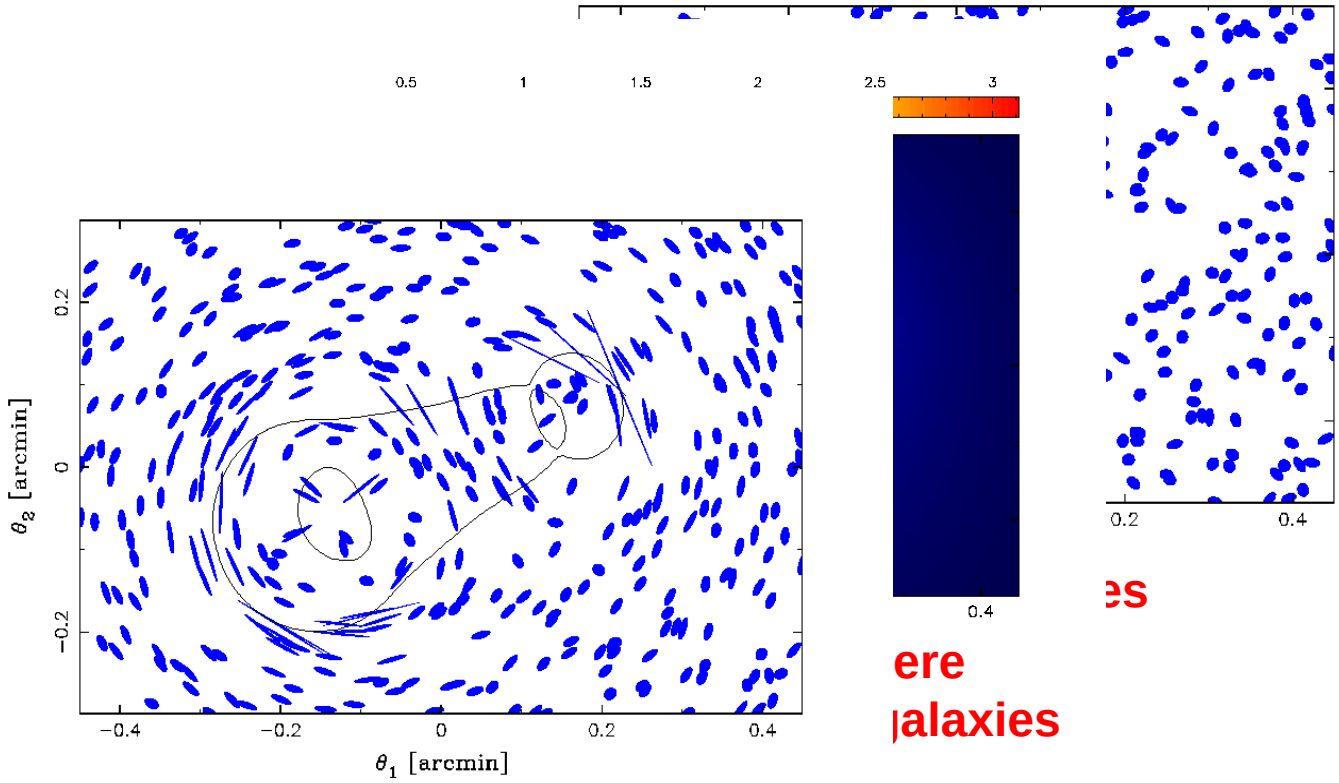

Coherent distortion pattern of background galaxies

It shows Dark Matter Distribution in Lensing Object

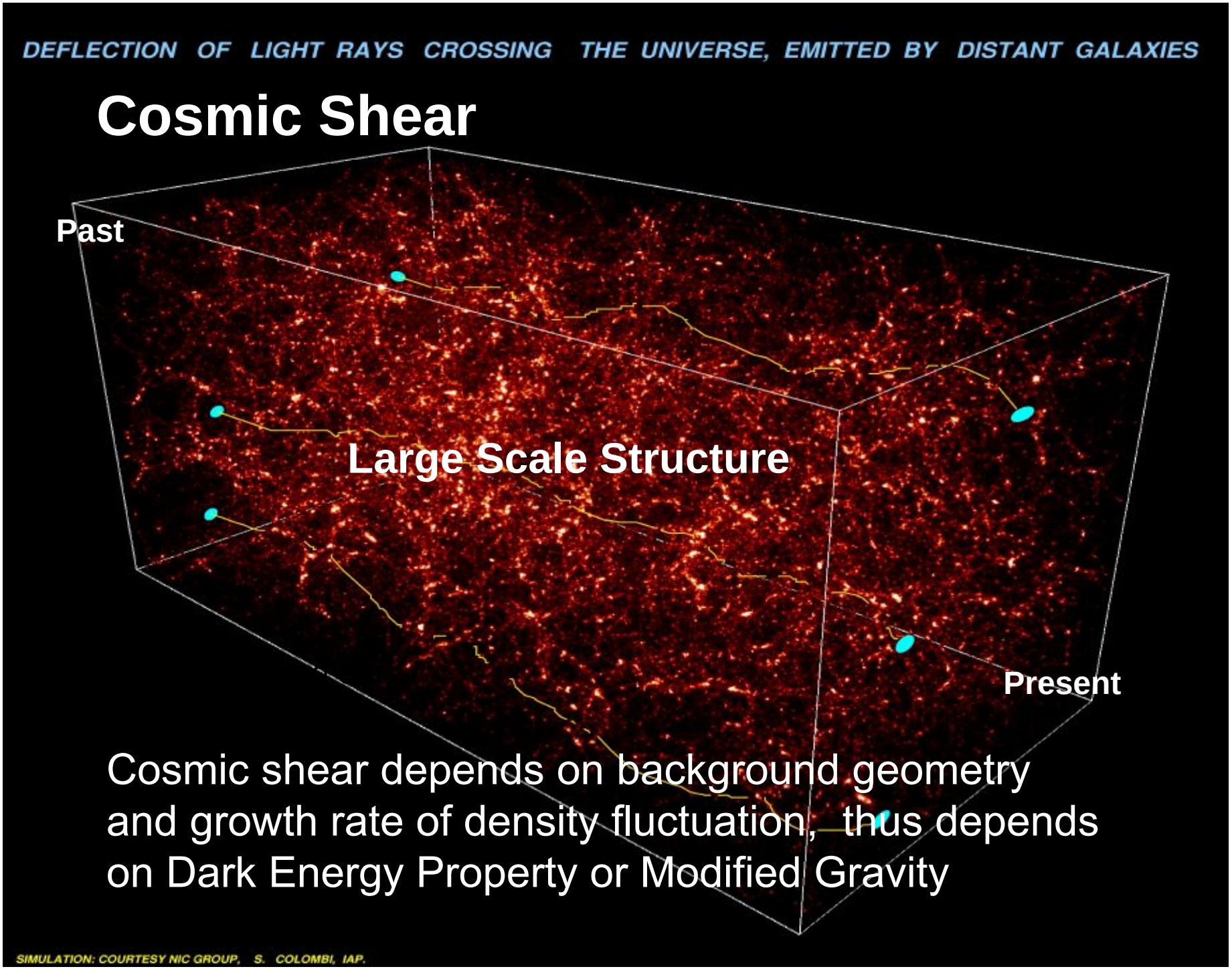
DEFLECTION OF LIGHT RAYS CROSSING THE UNIVERSE, EMITTED BY DISTANT GALAXIES
Cosmic Shear
Past
Large Scale Structure
Present
Cosmic shear depends on background geometry
and growth rate of density fluctuation, thus depends
on Dark Energy Property or Modified Gravity
SIMULATION: COURTESY NIC GROUP, S. COLOMBI, IAP.

Lens Mapping

$$\vec{\theta} = \vec{\beta} + \vec{\nabla}\psi(\vec{\theta})$$ ψ： Lens potential

$$\Delta_\theta \psi(\vec{\theta}) = 2\kappa$$

$$\kappa(\vec{\theta}) \equiv \frac{\Sigma(\vec{\theta})}{\Sigma_{cr}}, \Sigma_{cr} = \frac{c^2 D_s}{4\pi G D_l D_{ls}} \approx 0.35 \left(\frac{D}{1Gpc}\right)^{-1} g/cm^2$$

$$A(\vec{\theta}) = \frac{\partial \vec{\beta}}{\partial \vec{\theta}}(\vec{\theta}) = \delta_{ij} - \frac{\partial^2 \psi}{\partial\theta_i \partial\theta_j} = \begin{pmatrix} 1-\kappa+\gamma_1 & \gamma_2 \\ \gamma_2 & 1-\kappa-\gamma_1 \end{pmatrix}$$

convergence:

$$\kappa = \frac{1}{2}\Delta_\theta \psi = \frac{1}{2}(\psi_{,11} + \psi_{,22}) \propto \Sigma$$

shear:

$$\gamma = \gamma_1 + i\gamma_2 \equiv \frac{1}{2}(\psi_{,11} - \psi_{,22}) + i\psi_{,12}$$

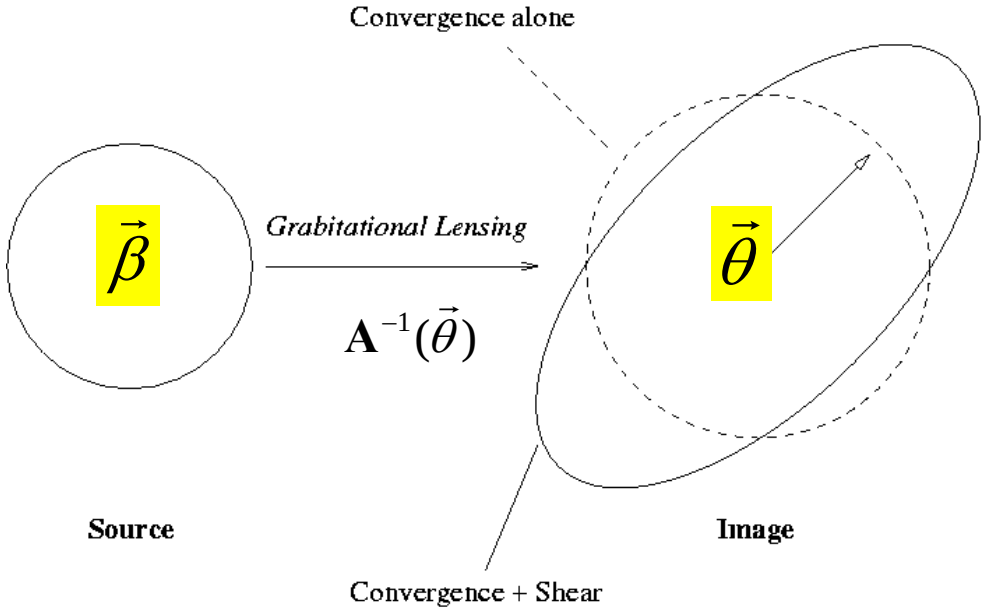

Observation of shear

(1) Measure 2nd order moments of brightness distribution of individual galaxies (IMCAT)

$$Q_{ij} = \int d^2\theta\, W(\theta)\theta_i\theta_j I(\vec{\theta})$$ w(θ): weight function

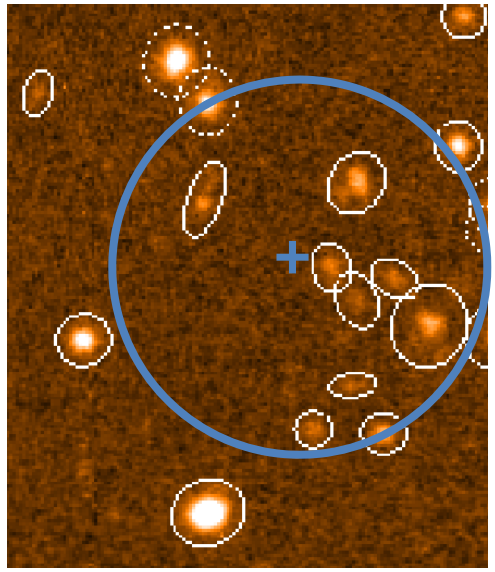

(2) Calculate ellipticity

$$\vec{\chi} := \left(\frac{Q_{11}-Q_{22}}{Q_{11}+Q_{22}} \quad \frac{2Q_{12}}{Q_{11}+Q_{22}} \right) \rightarrow \frac{a^2-b^2}{a^2+b^2}\left(\cos(2\varphi) \quad \sin(2\varphi)\right)$$

$$\Rightarrow \quad \vec{\chi}_{obs} \approx \vec{\chi}_{\text{intrinsic}} + 2\vec{\gamma} \qquad (|\gamma|,|\kappa| << 1)$$

(3) Assume that sources are statistically round $< \vec{\chi}_{\text{intrinsic}} >= 0$

$$\Rightarrow \quad < \vec{\chi}_{obs} > = 2 < \vec{\gamma} > + O\left(\frac{\sigma_{\text{int}}}{\sqrt{N}} \right)$$

Direct, unbiased estimator for the gravitational shear

*) In reality we need PSF correction

Weak lensing mass reconstruction

Image distortion (gravitational shear) field

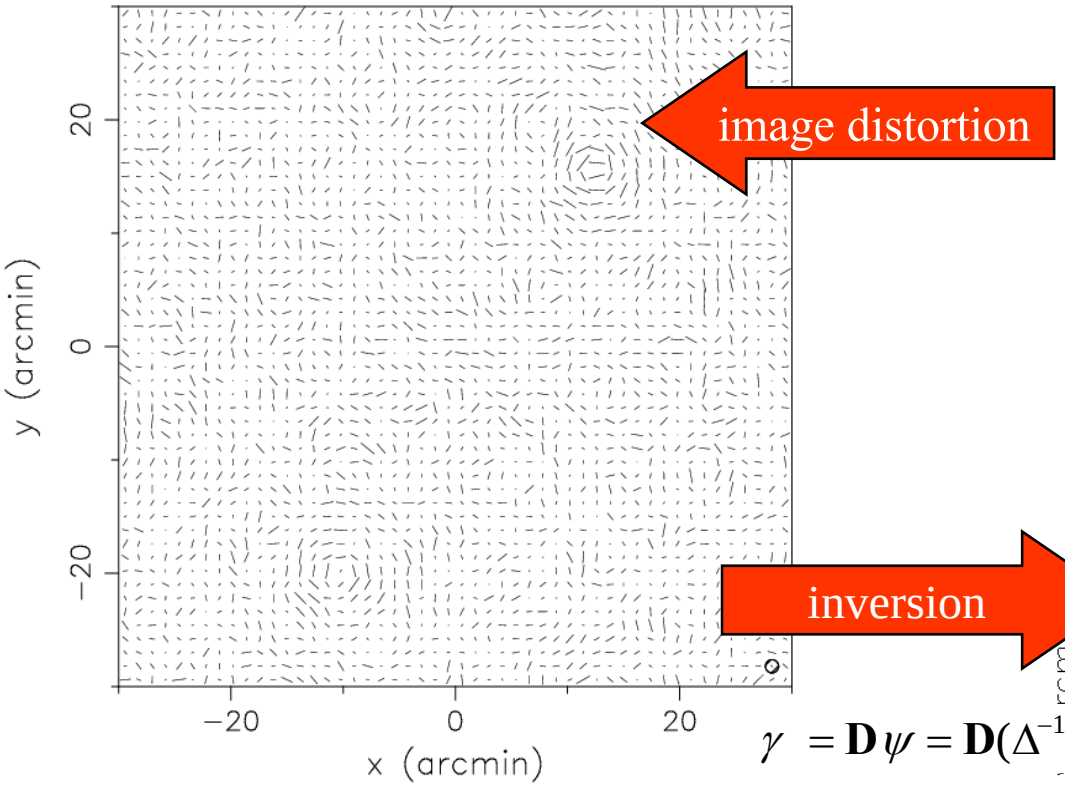

image distortion

inversion

$$\gamma = \mathbf{D}\psi = \mathbf{D}(\Delta^{-1}2\kappa)$$

Observation

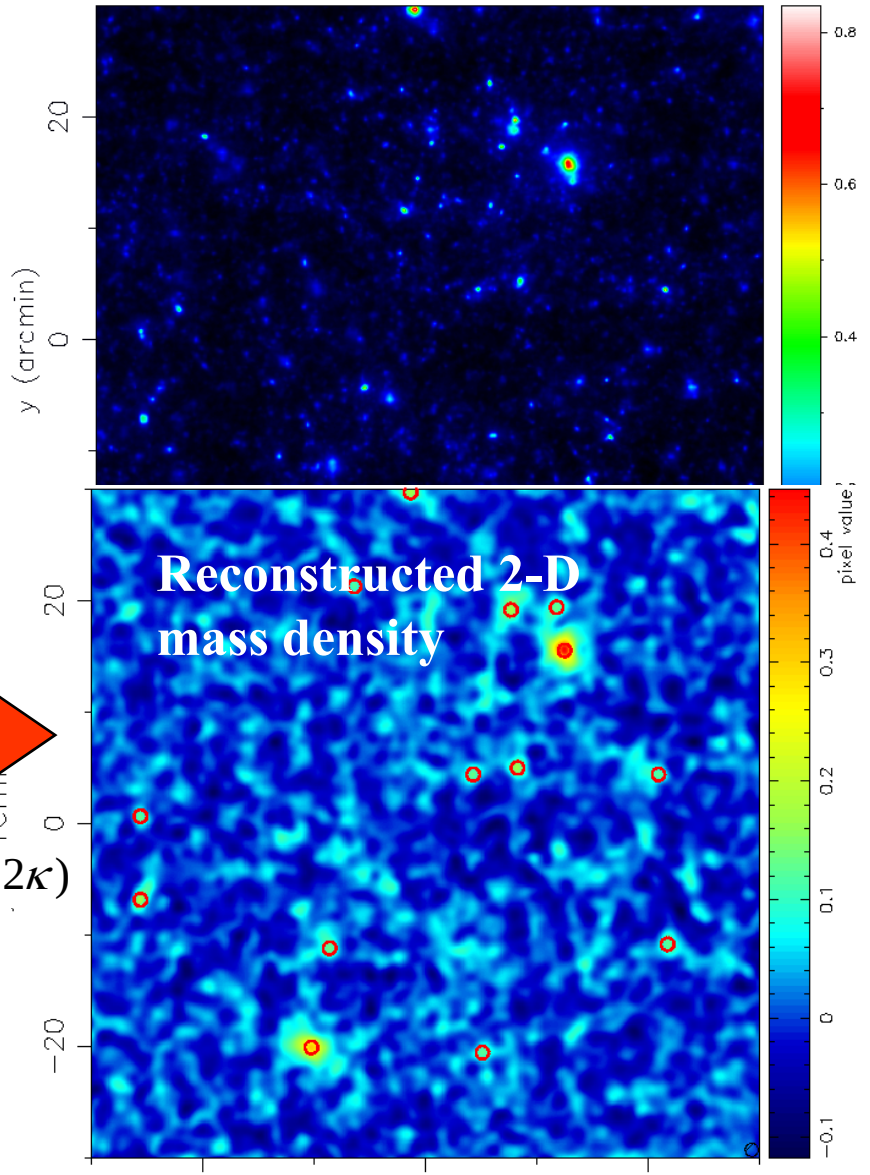

Weak lensing analysis of clusters of galaxies

- A1689

  Strong(HST)+weak(Subaru) observation

  NFW profile with abnormally high concentration parameter

- Coma cluster

  toward observational determination of mass function of substructures

- Colliding clusters

  evidence for DM

Abell 1689

Very Massive cluster @z=0.183

- $2\times10^{15}M_{sun}$, r_{vir}=2Mpc
- Einstein radius (≈50'' for z=3) ⇔typically 15''
- *X-ray Temp* 9keV (XMM: Anderson & Madejski 2004)
- Vel. dispersion σ_{1D}=2400km/s (Targue et al. 1990) or 1400km/s (Girardi et al. 1997)

High resolution N-body simulations of CDM structure formation predict an universal profile for cluster

NFW profile

$$\rho_{NFW}(r) \propto \frac{1}{r(r+r_c)^2} = \frac{1}{r_{200}^3 x(x+1/c)^2}$$

$\boxed{c = r_{200}/r_c}$:concentration parameter

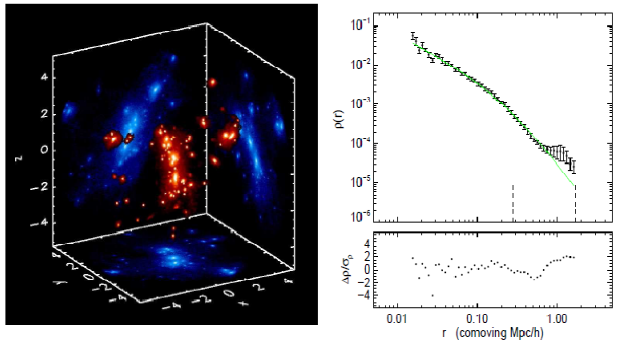

Subaru/S-Cam and HST/ACS observation of A1689

Revealing 106 lensed multiple images of 30 background galaxies (Broadhurst et al. 2004)

S-Cam (wide field⇒weak lensing)

ACS (high resolution⇒ Strong lensing)

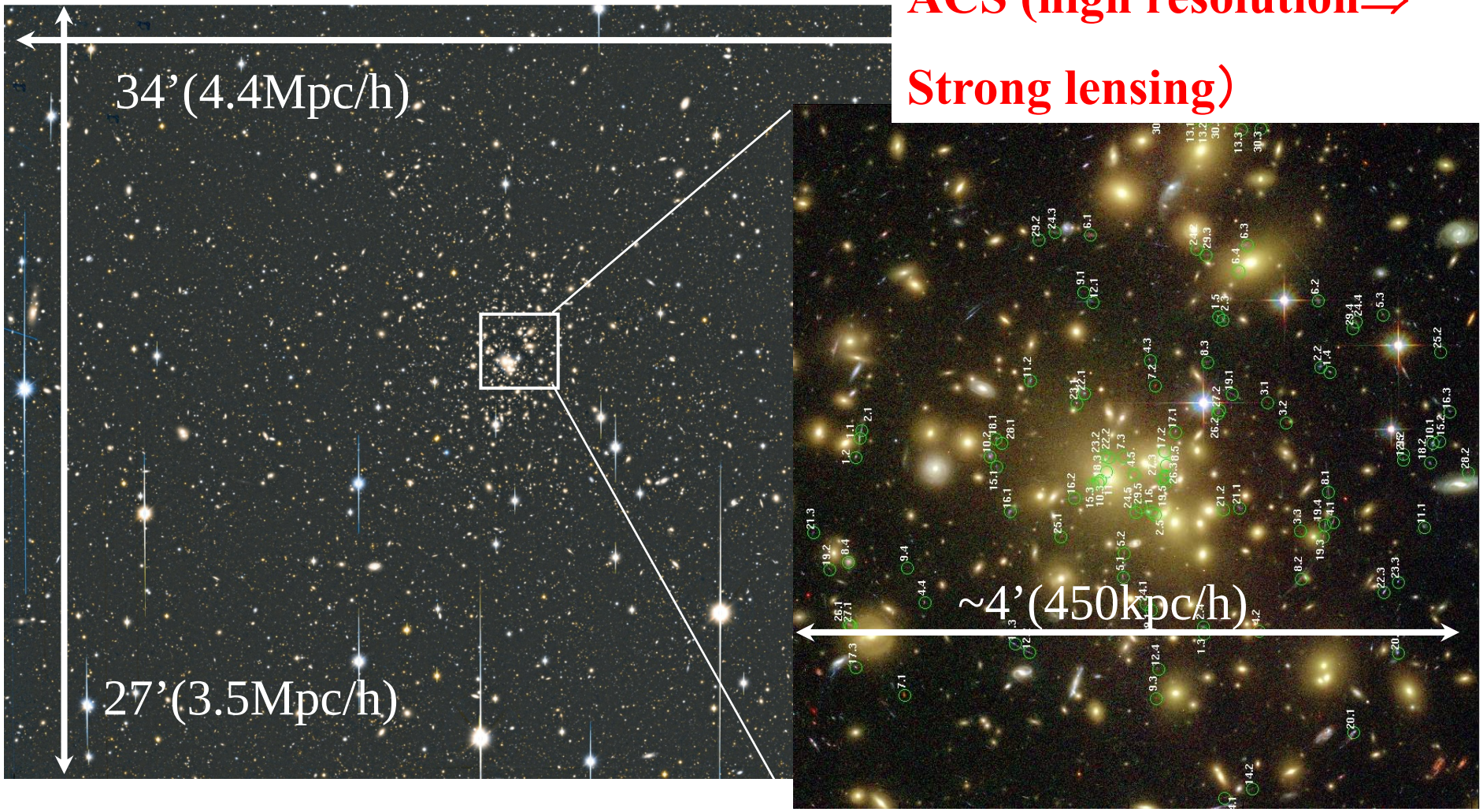

Isocontour of 2D mass density

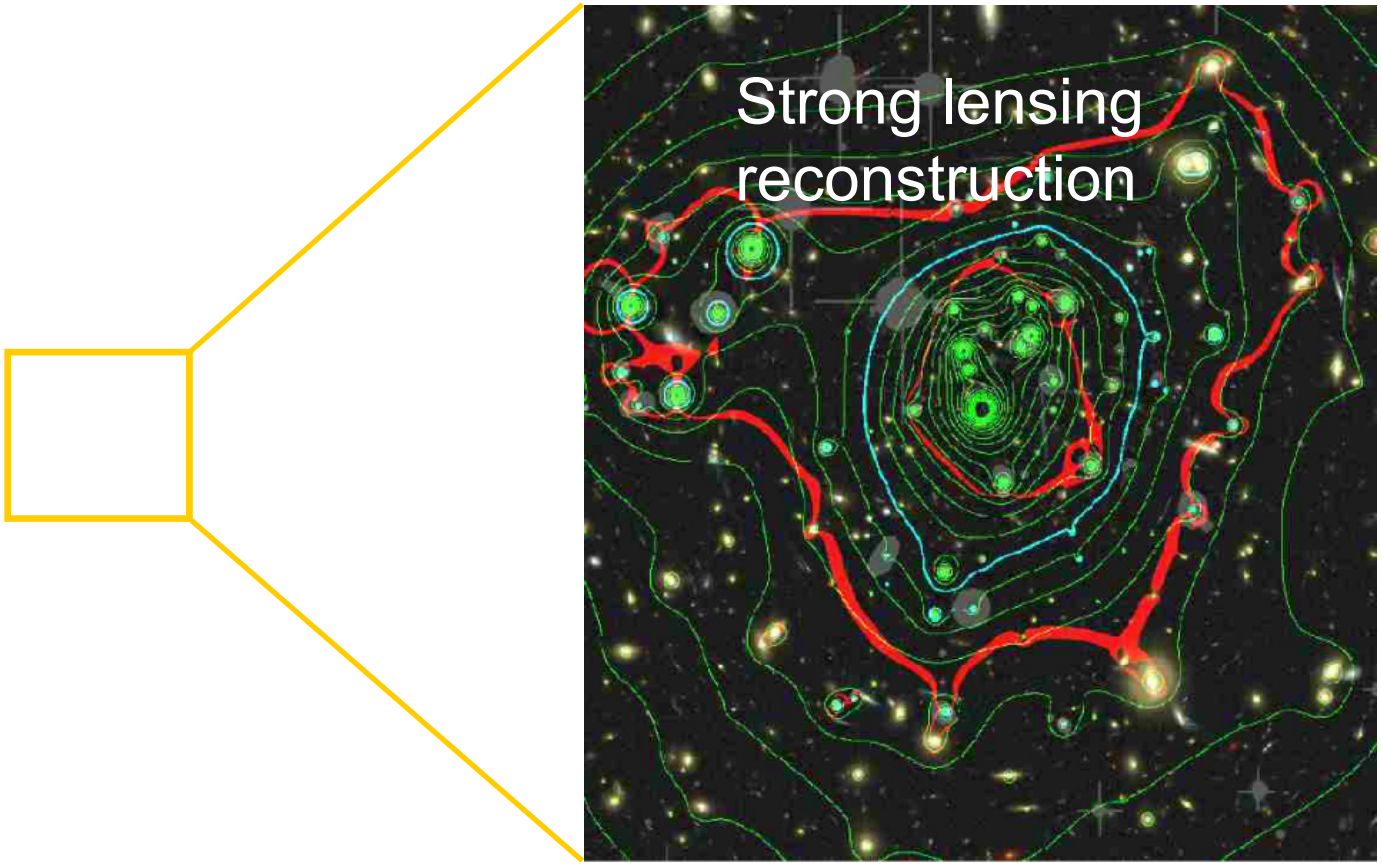

Reconstructed Mass Profile

Strong lensing(HST)+weak lensing (Subaru) analysis of A1689

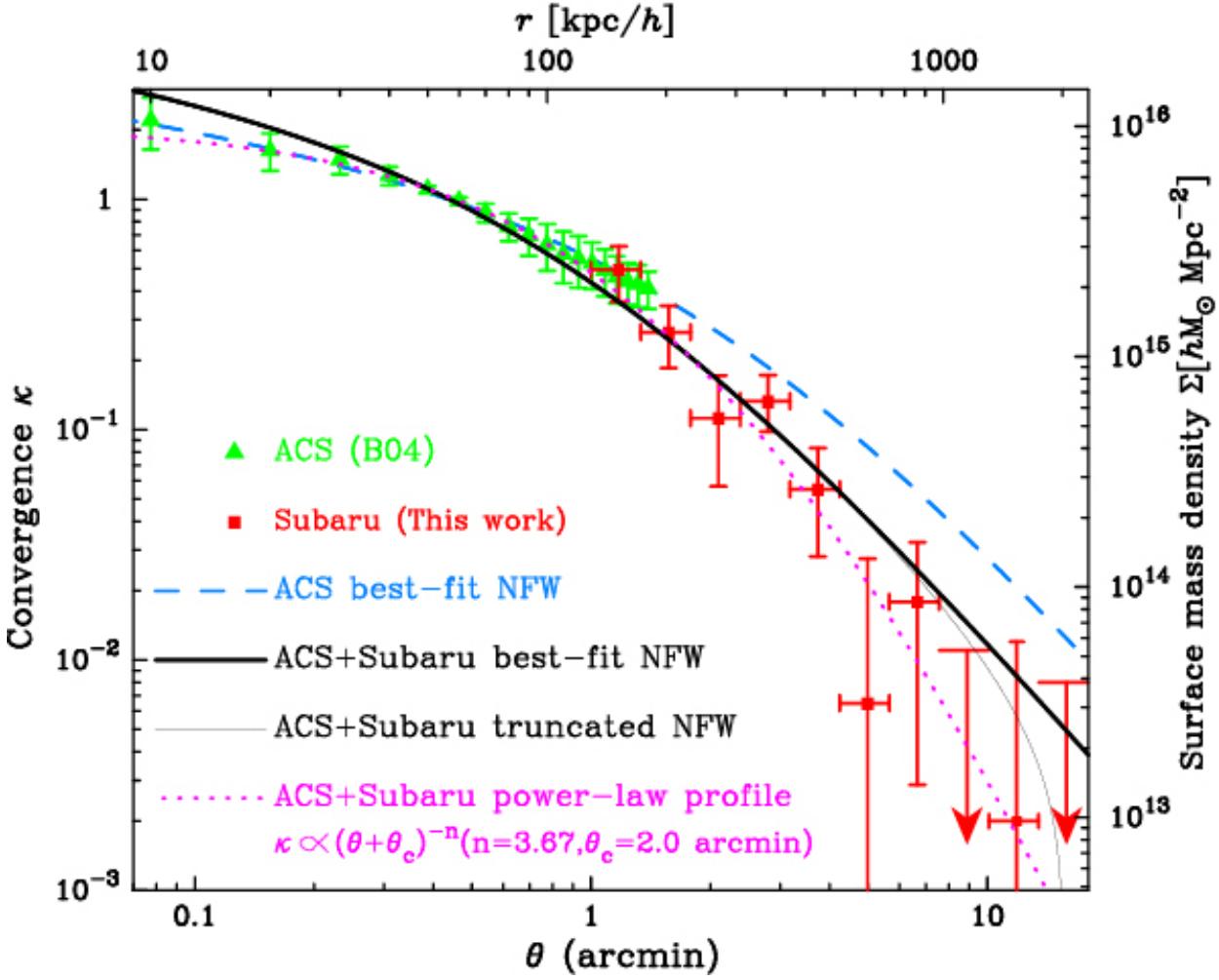

22 data points

●Best-fit NFW

$$M_{\rm vir} = 1.7^{+0.05}_{-0.05} \times 10^{15} M_{\rm s}$$

$$r_{\rm vir} = 2.0 \pm 0.02 {\rm Mpc}/h$$

$$c_{\rm vir} = 13.7^{+1.4}_{-1.1}$$

K.Umetsu and T. Broadhurst 2008

c_vir=12.7±1(stat.) ±2.8(systematic)

Contradiction to prediction $\Leftrightarrow c_{simulation} \approx 5 \pm 1$

Distribution of Concentration parameter predicted by N-body simulations

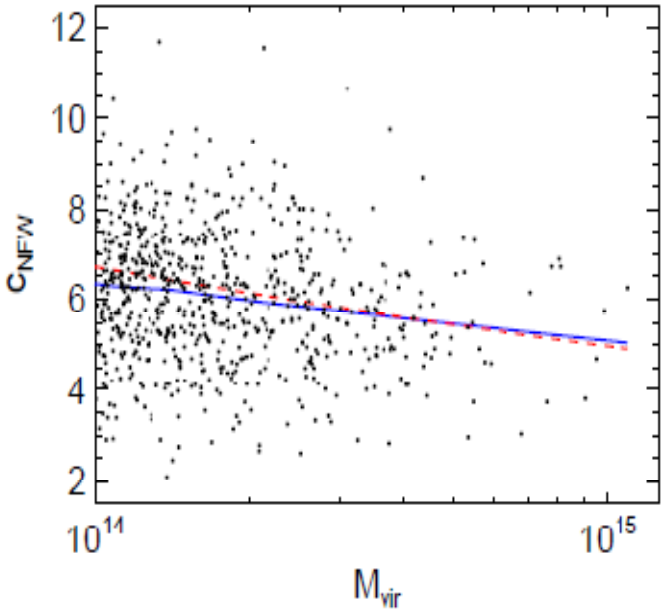

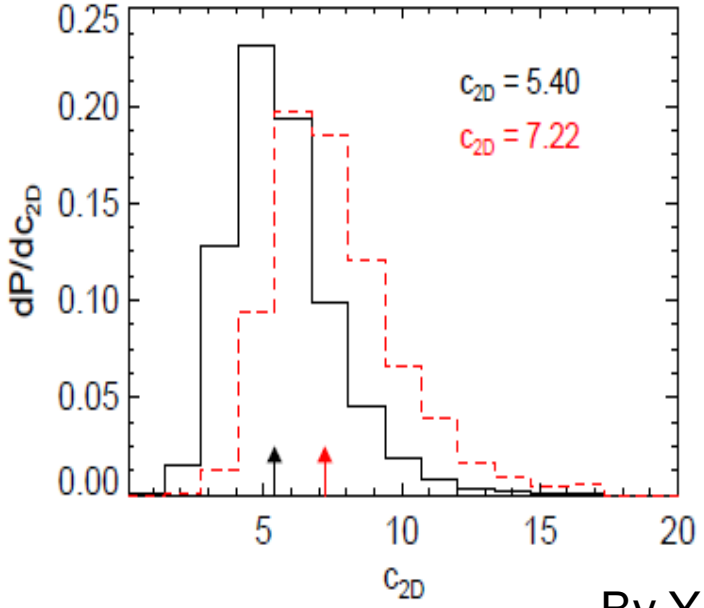

By Y. P. Jing

$$\rho_{NFW}(r) \propto \frac{1}{r(r+r_c)^2} = \frac{1}{r_{200}^3 x(x+1/c)^2}; \quad x = r/r_{200}$$

r_c : Scale radius

r_{200} : Virial radius within which the mean mass density is 200 × the critaical density

$\boxed{c = r_{200}/r_c}$ Concentration parameter

NFW halo mass-concentration degeneracy

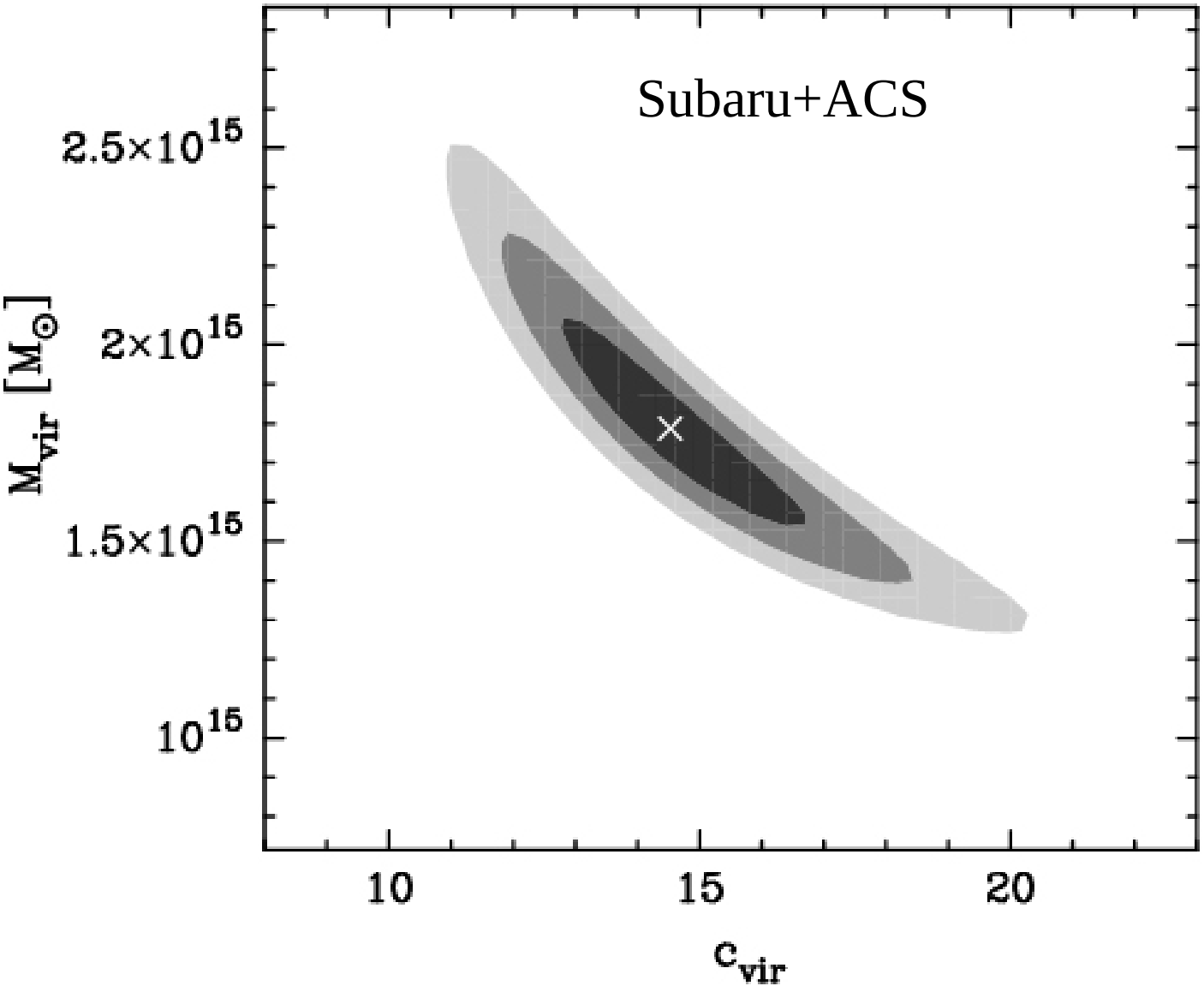

Is A1689 special ?

Weak lensing analysis of 30 nearby clusters (0.14 < z < 0.3)
by Subaru/Suprime-cam

The sample is taken from POSAT All sky survey (L_X[0.1-2.4keV]>3 × 10^44 erg/sec)

Example: mage and Mass map of A209 at z=0.209

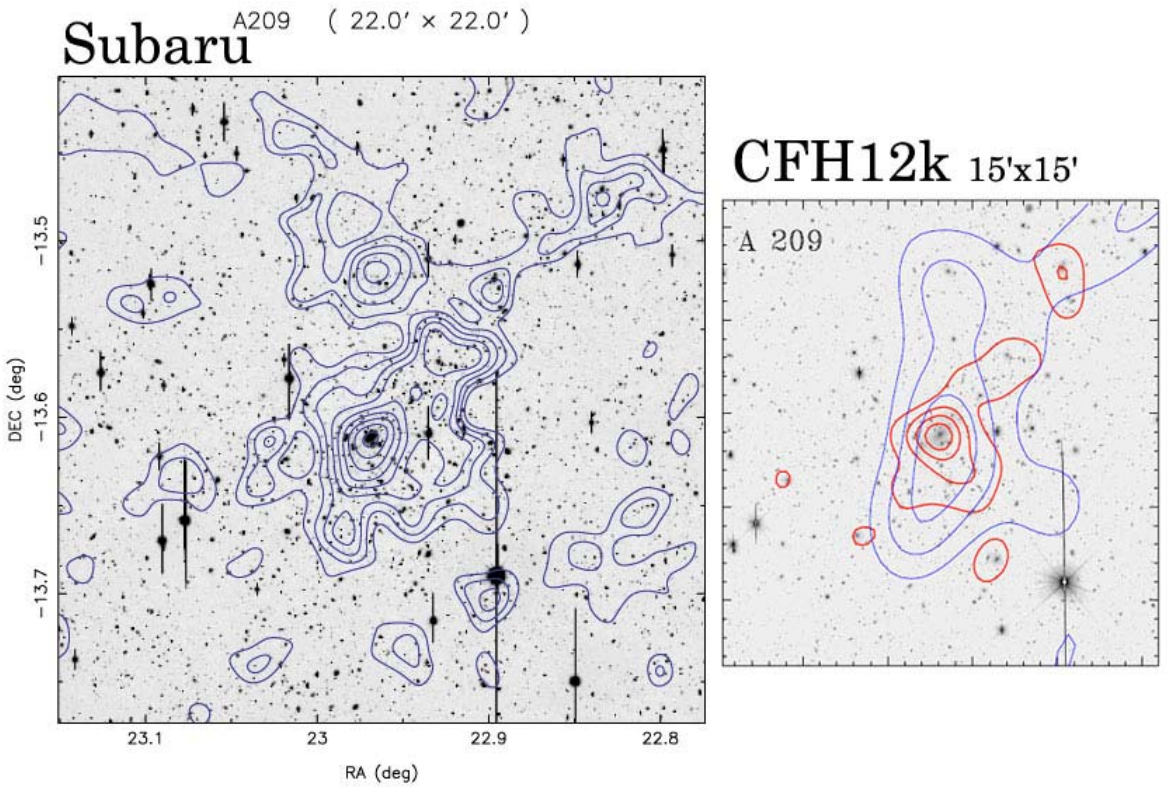

Concentration-mass relation for 20 clusters(0.14<z<0.3)

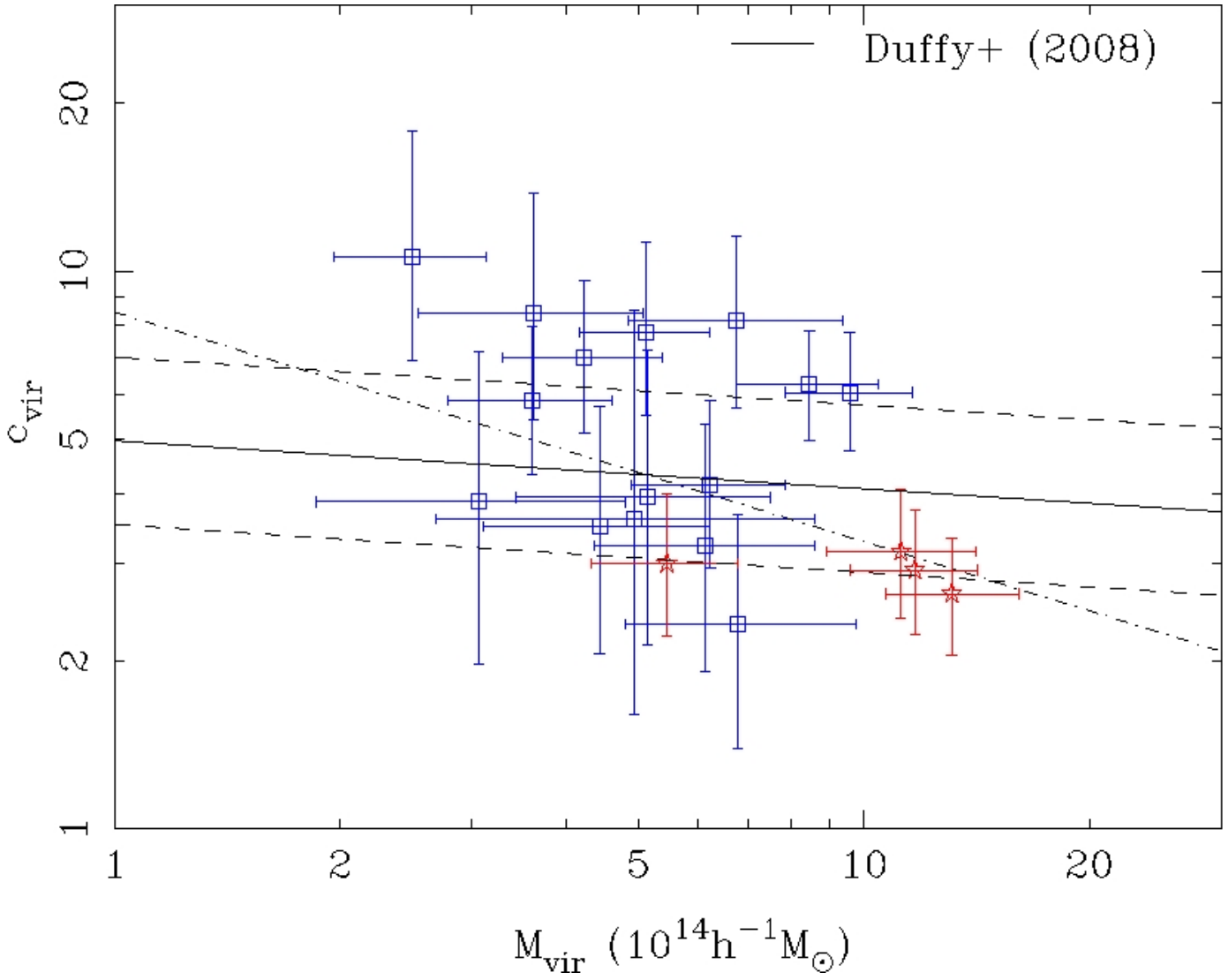

Result of Observation shows
bimodal distribution of concentration parameters

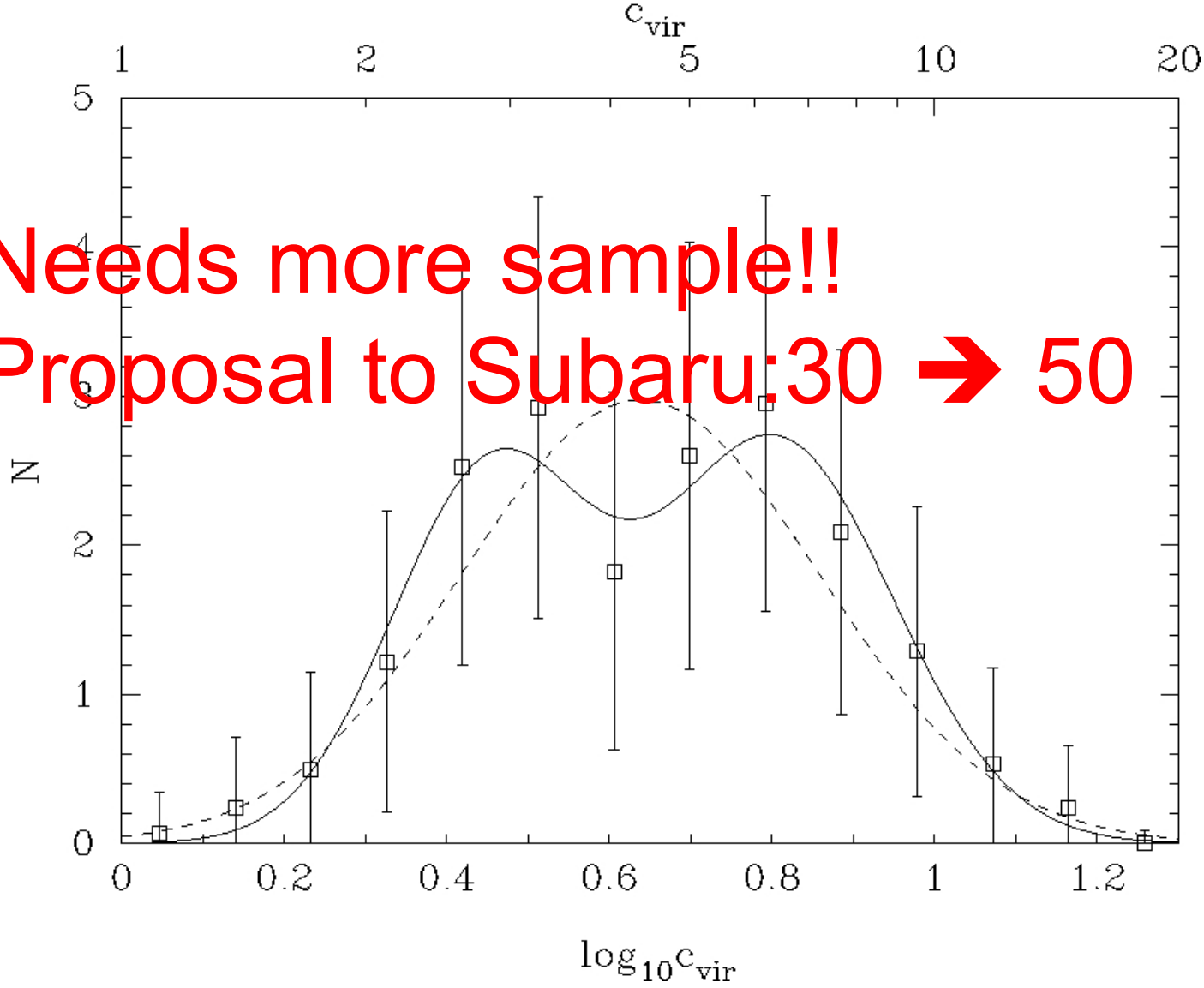

Needs more sample!!
Proposal to Subaru:30 ➔ 50

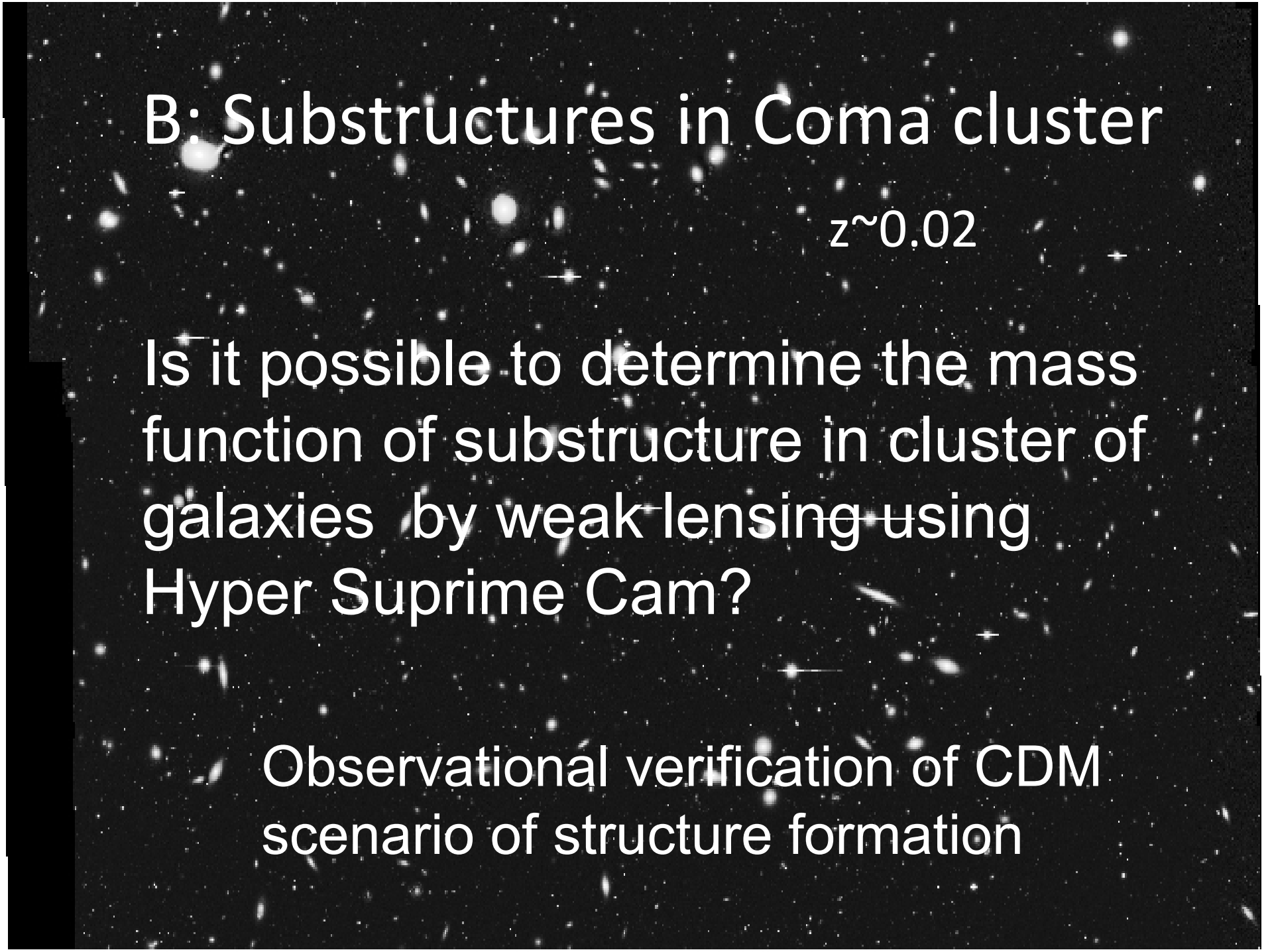

B: Substructures in Coma cluster

z~0.02

Is it possible to determine the mass function of substructure in cluster of galaxies by weak lensing using Hyper Suprime Cam?

- Observational verification of CDM scenario of structure formation

Suprime-Cam on Subaru

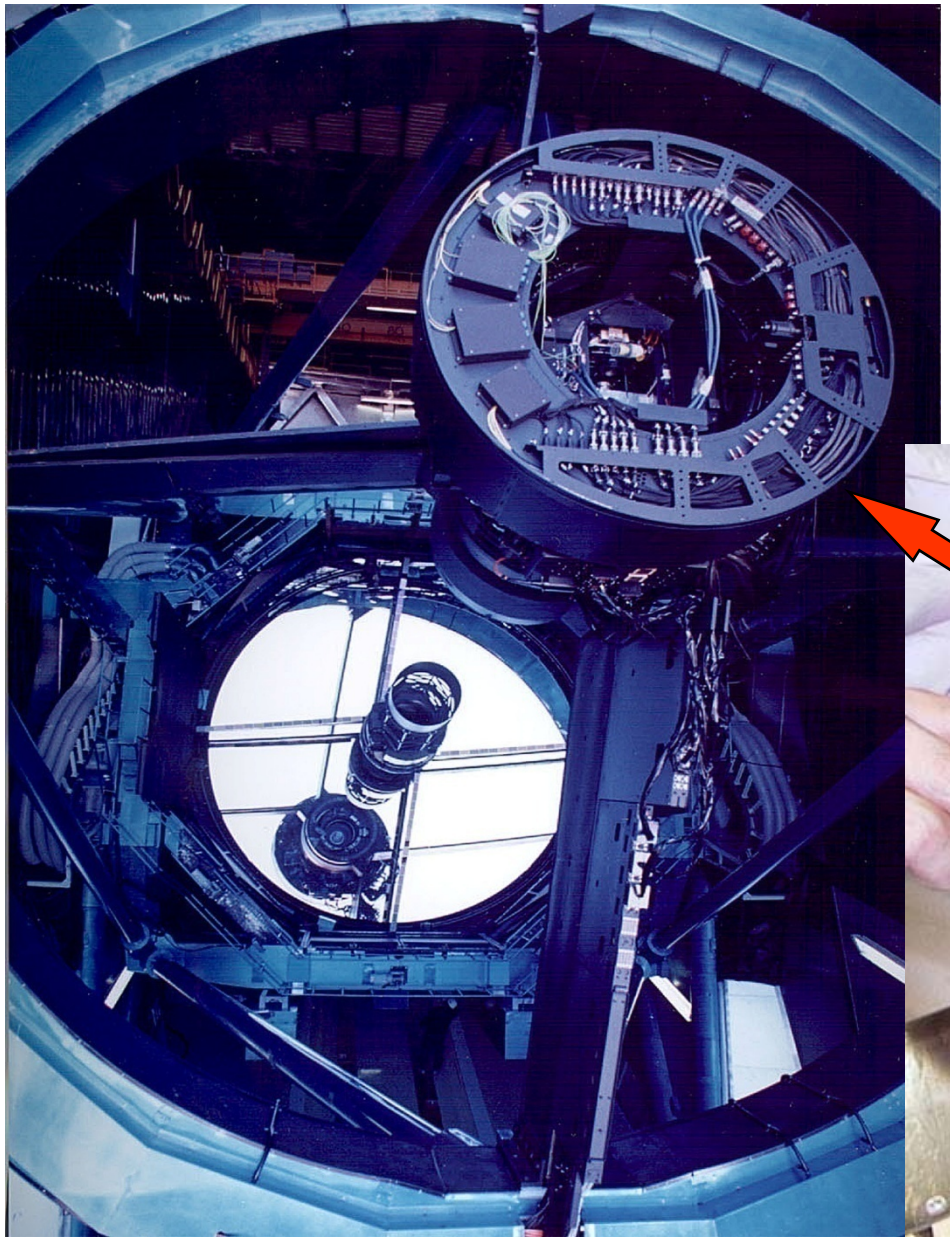

- Prime Forcas Camera
- 34’×27’ FOV

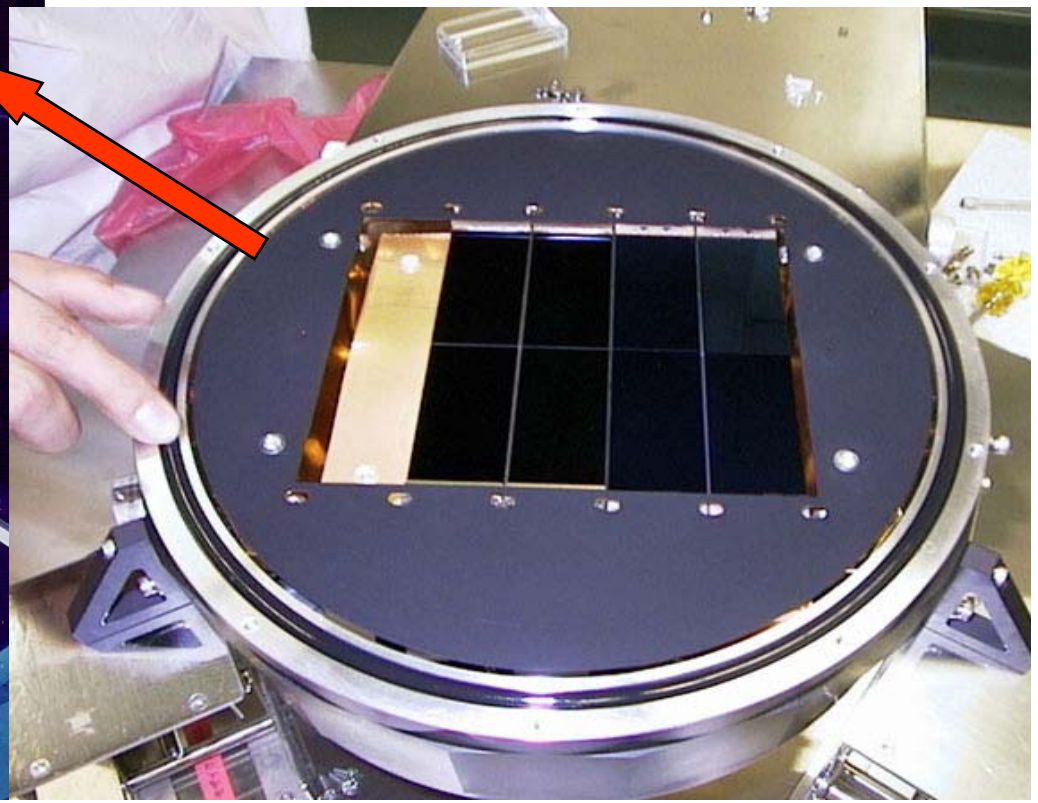

Hyper Suprime-Cam for Subaru

High-z Galaxy Survey for BAO and cosmic shear observations

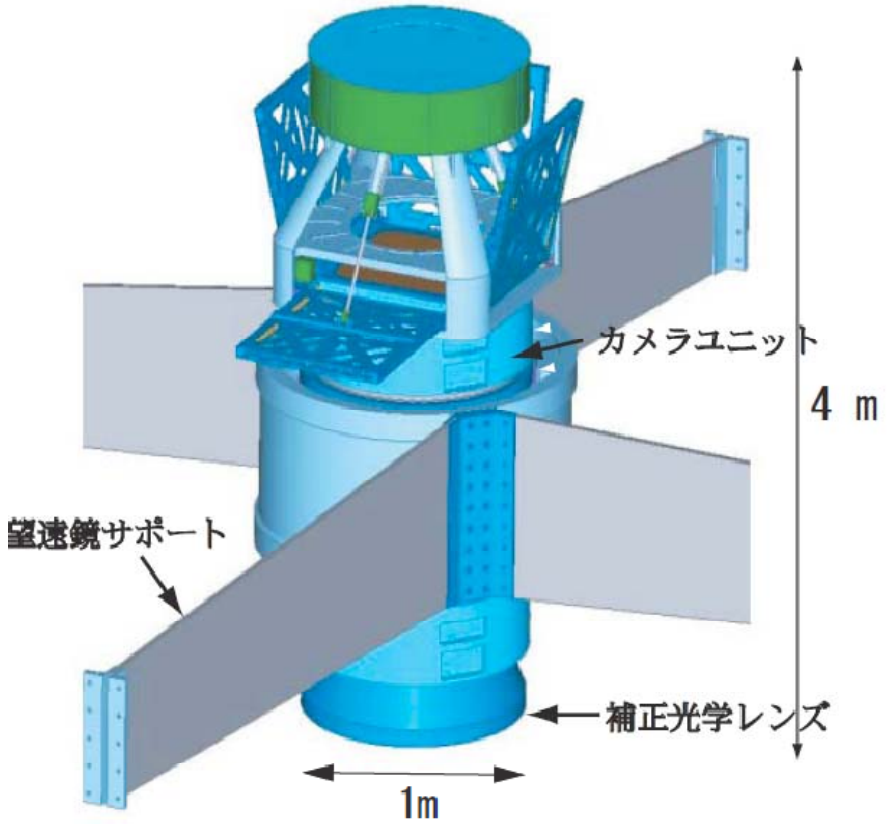

- Wide FOV (~10 times of S-Cam)
- High resolution（3 times better than the present at 1 micrometer）

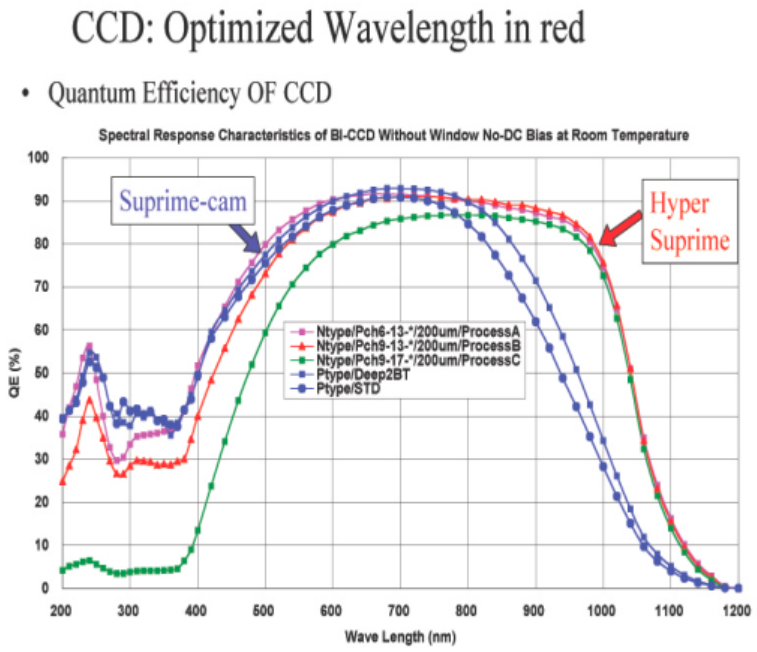

FOV of HyperSuprime

（80million chips

→1.6billion chips）

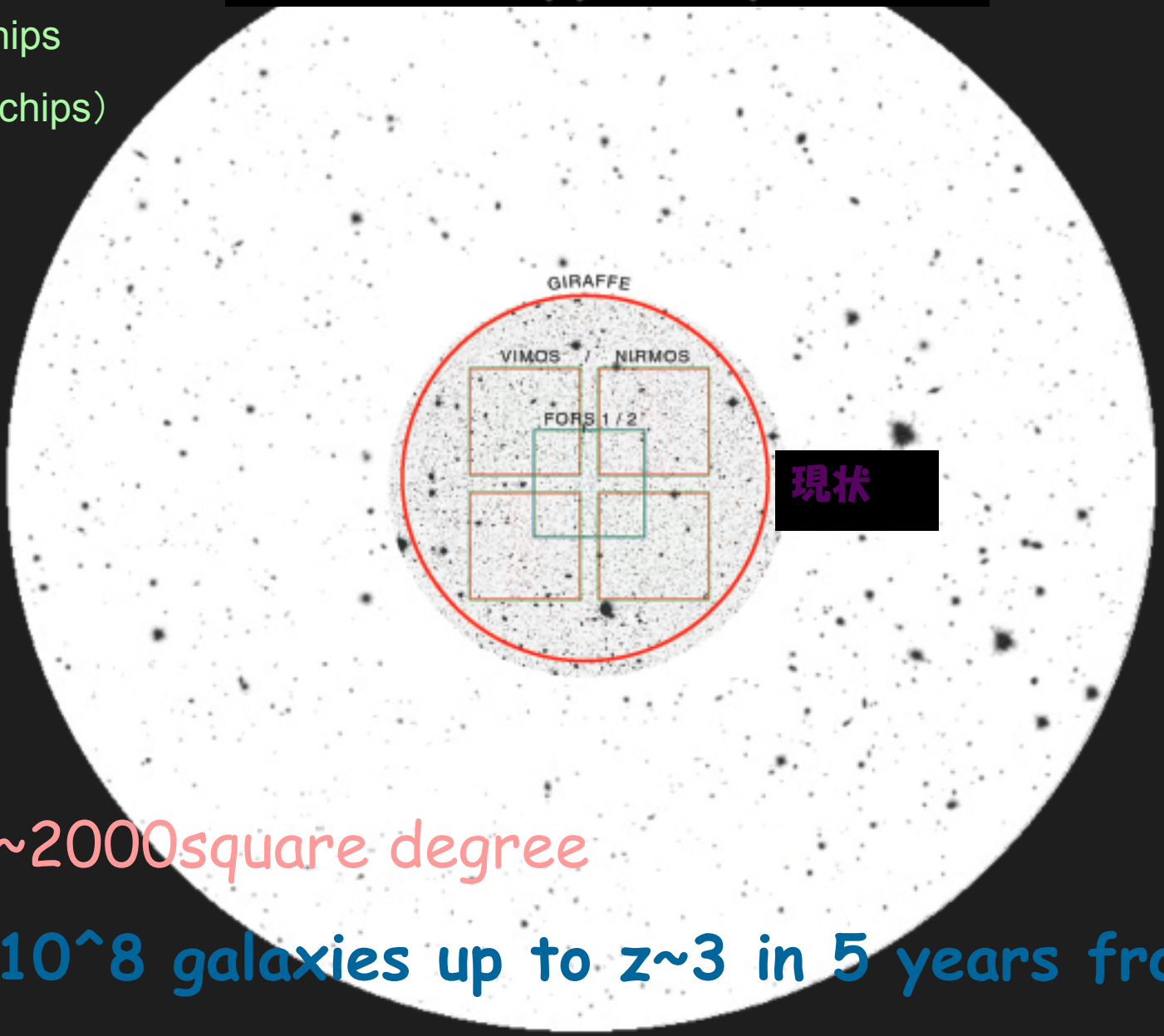

現状

1000 ~2000square degree

1.5×10^8 galaxies up to z~3 in 5 years from 2011

Observations by Hyper Suprime-Cam

- Cosmic shear
- BAO

These are two main observations proposed, but we can make the following observations as well

By observing very close clusters to see directly dark matter subhalos in clusters which reveal the details of structure formation

Quasar statistics using a complete quasar survey up to z~3 to constrain the dark energy properties as well as evolution of number density of lensing galaxies

SDSS sample (z<2) is too shallow to have useful constraints

As a preliminary study we made weak lensing analysis of small region in coma cluster by old S-Cam(present S-Cam has new CCD)

Two R-band image data from SMOKA(Subaru Archive Data)

Central region of r<30’ from CD galaxy NGC4874 (42min)
Outskirts region of r~30-60’ (16min)

Source galaxies 20-25 AB mag

~23 arcmin^-2 background galaxies

Density profile of main cluster

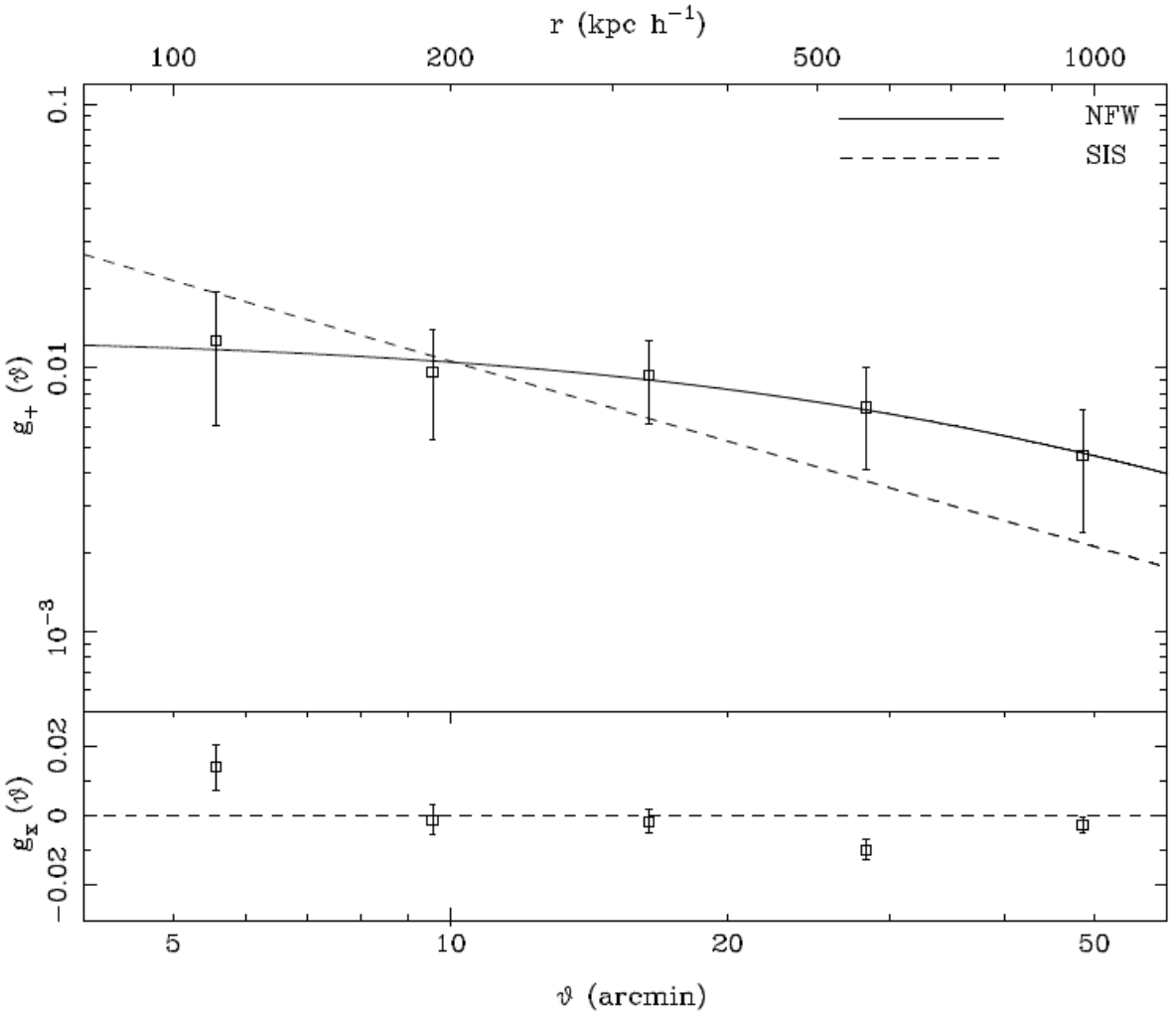

Fig. 1.— Profiles of tangential shear component, g_+, and the 45 degree rotated component, $g_\times$. The solid and dashed lines are the best-fitting NFW and SIS model, respectively

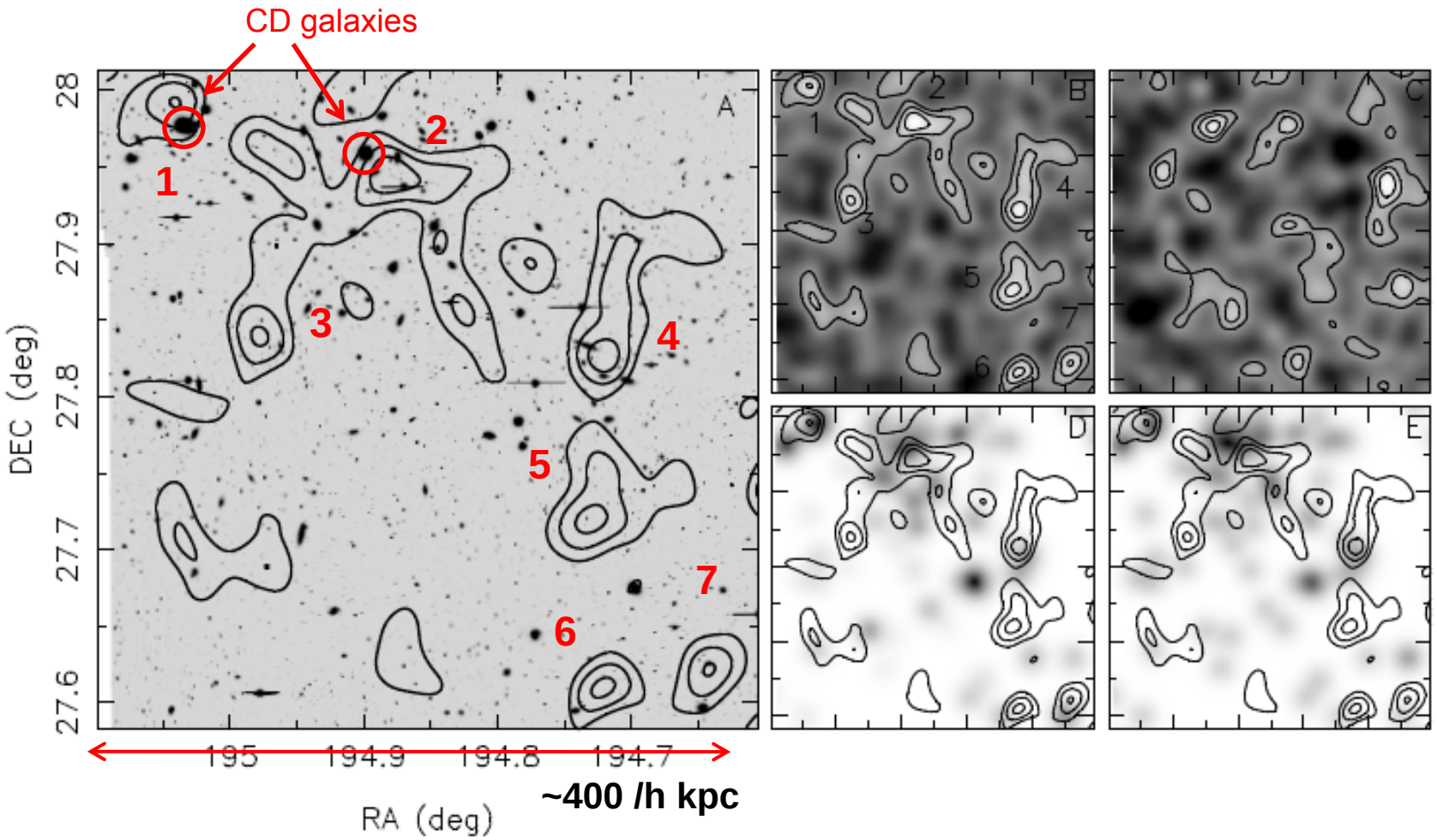

Fig. 2.— The panel A is Subaru R_c-band image of the central 26′. × 26′. cluster region. Two cD galaxies (NGC 4874 and NGC 4889) are located around the northeast boundary. Overlaid are contours of the reconstructed projected mass distribution, spaced in a unit of 1σ reconstruction error. The Gaussian FWHM is 2′.00. The panels B and C are the lensing *kappa* and b-mode fields. The identified subclumps are labeled in the panel B. The panels D and E are cluster luminosity and density distributions in SDSS i'-band smoothed to the same angular resolution of the mass map, respectively.

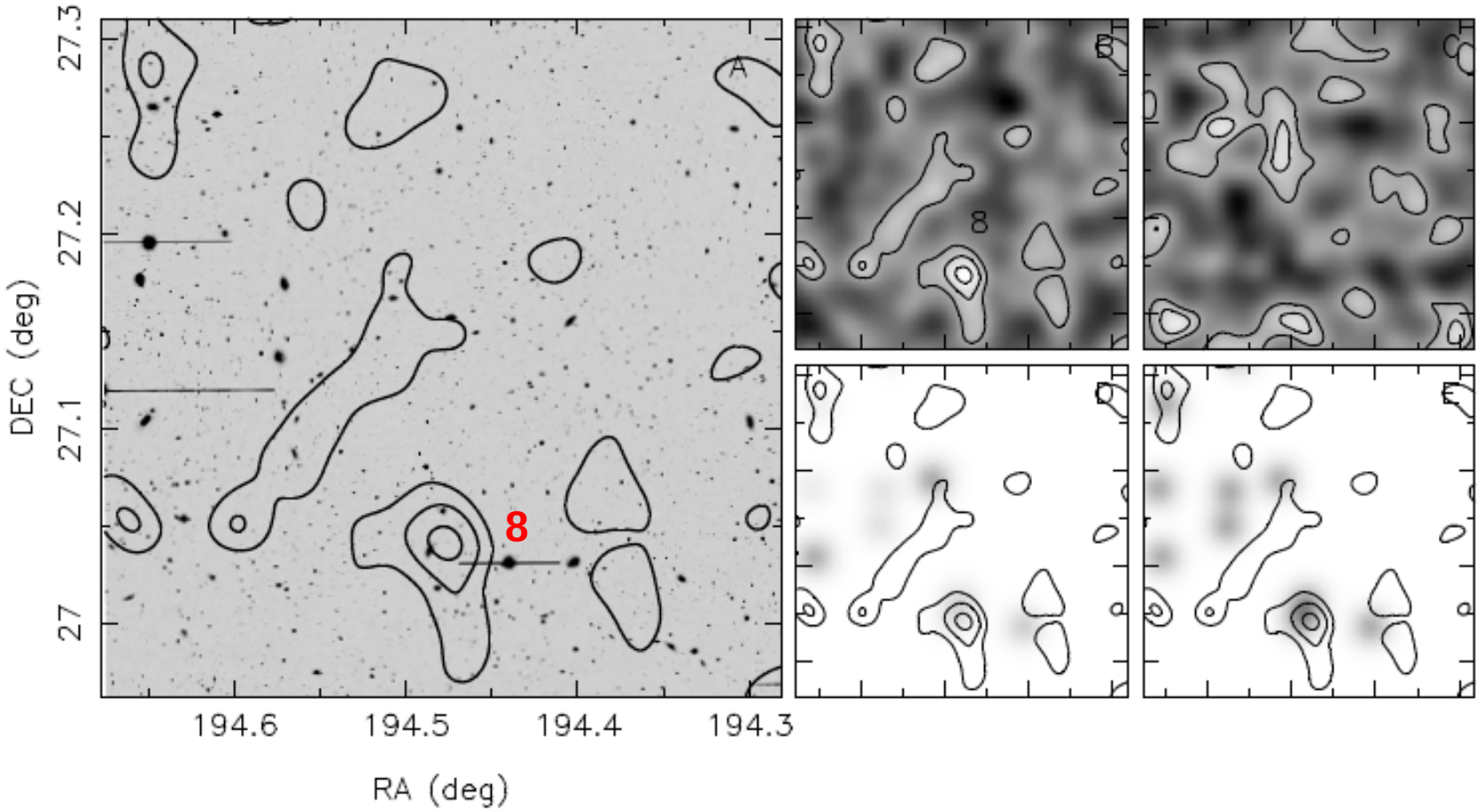

Fig. 3.— The panel A is Subaru R_c-band image of the outskirts $21' \times 21'$ cluster region. Overlaid are contours of the reconstructed projected mass distribution, spaced in a unit of 1σ reconstruction error. The Gaussian FWHM is $2'.00$. The panels B and C are the lensing *kappa* and b-mode fields. The identified subclumps are labeled in the panel B. The clump 8 is far $\sim 58'$ from cD galaxy NGC4874. The panels D and E are cluster luminosity and density distributions in SDSS i'-band smoothed to the same angular resolution of the mass map, respectively.

Projected Mass for Subclump candidates

ID	$M_{2D}(< 30h^{-1}\mathrm{kpc})$ $(10^{12}h^{-1}M_{\odot})$
(1)	(2)
1	4.23 ± 1.94
2	5.01 ± 1.65
3	4.16 ± 1.52
4	4.40 ± 1.52
5	3.29 ± 1.52
6	4.83 ± 1.63
7	3.61 ± 1.58
8	5.15 ± 1.82

We measured the projected mass for eight subclump candidates within a circular aperture of radius 30kpc, considering the uncertainty of the central position of subclump. The mean 2D mass yields $\langle M_{2D} \rangle = (4.33 \pm 0.58) \times 10^{12}h^{-1}M_{\odot}$. The 2D mass of the SIS model of subhalo is given by $M_{2D}^{(SIS)}(\theta) = 3.5 \times 10^{12}h^{-1}M_{\odot}(\sigma_v/400\mathrm{km/s})^2(\theta/30\mathrm{kpc})$, where σ_v is the velocity dispersion and we employ the velocity dispersion of cD galaxy $\sim 200-400$km/s (e.g. Smith et al. 2000). It indicates that cluster have some subhalos whose masses ($> 10^{12}h^{-1}M_{\odot}$) is at the order of the mass of cD galaxy halos.

We found five subhalos and two cD galaxy halos in the central data ($r \lesssim 30'$) and one halo in the outskirts data ($30' \lesssim r \lesssim 60'$). There is a difference of the halo number for the radius, which might support the numerical simulation result (e.g De Lucia et al. 2004;Gao et al 2004) that the number of substructure increases the radius decreases. Compensating the limitation of our data region, we roughly calculate the number of subhalos within the radii $r_{\rm rvir}$ and r_{200}. If we assume that there are five ($r \lesssim 30'$) and one ($30' \lesssim r \lesssim 60'$) subhalo in the area corresponding to our data, the halo number is estimated by $\pi(r_{\rm vir}^2 - 30'^2)/{\rm area}_{\rm outskirts} + 5 \times (\pi 30'^2/{\rm area}_{\rm center}) + 2$. And the Poisson noise for distributions is applied and the halo number detected by weak lensing analysis is expected to be $N_{\rm sub}(< r_{\rm vir}) = 46 \pm 30$ and $N_{\rm sub}(< r_{200}) = 30 \pm 15$. If the typical halo mass is the best-fit value $\langle M_{\rm sub} \rangle = 4.18 \times 10^{12} h^{-1} M_\odot$ obtained from fitting of the stacked tangential profile, the total substructure mass within the viral radius account for $\sim 22 \pm 14$ and 19 ± 10 percents of total cluster masses $M_{\rm vir}$ and M_{200}, respectively. Although the total mass fraction invested in subhalos is little agreement among the results in the literature (e.g. De Lucia et al. 2004; Natarajan et al. 2007, Gao et al. 2004), most authors estimate 5 -20 percent. Our result is in board agreement with the numerical simulations. A galaxy-galaxy lensing study (Natarajan et al. 2007) represented that the mass faction of cluster substructures ranges $10 - 20\%$, which coincides with our result.

More Observation !
Hyper Suprime-Cam!

2. HOLICs

Motivations

There are many highly distorted images of faint and distant galaxies which have not used or inaccurately used in the weak lensing analysis

How can one make use of these images in the weak lensing analysis?

What is the description of these images other than second order moments?

Shaplet or Higher order moments

How to find useful combinations of higher order moments

Quadrupole moments

$$Q_{ij} \propto \int d^2\theta\, I(\theta)\theta_i\theta_j$$

$$\chi \equiv \frac{Q_{11} - Q_{22} + 2iQ_{12}}{Q_{11} + Q_{22}} \quad \Rightarrow \quad \chi^{(s)} \approx \chi - 2\gamma$$

Spin-2 combination

Higher-order moments

Find combinations having definite spin

HOLICs (Higher Order Lensing Characteristics)

Definition of HOLICs

$$Q_{ijk} \equiv \frac{\int d^2\theta\, q_I[I(\boldsymbol{\theta})]\Delta\theta_i\Delta\theta_j\Delta\theta_k}{\int d^2\theta\, q_I[I(\boldsymbol{\theta})]},$$

$$Q_{ijkl} \equiv \frac{\int d^2\theta\, q_I[I(\boldsymbol{\theta})]\Delta\theta_i\Delta\theta_j\Delta\theta_k\Delta\theta_l}{\int d^2\theta\, q_I[I(\boldsymbol{\theta})]}.$$

$$\zeta \equiv \frac{(Q_{111}+Q_{122})+i(Q_{112}+Q_{222})}{\xi},$$

$$\delta \equiv \frac{(Q_{111}-3Q_{122})+i(3Q_{112}-Q_{222})}{\xi},$$

Spin-1

Spin-3

$$\xi \equiv Q_{1111}+2Q_{1122}+Q_{2222}$$

Spin-0

What kind of lensing properties related with HOLICs?

Relation between Source HOLICs and image HOLICs

Source octo-pole moment

$$Q_{ijk}^{(s)} \propto \int d^2\beta \; I(\beta)\Delta\beta_i\Delta\beta_j\Delta\beta_k$$

Lens equation: $\boldsymbol{\beta} = \boldsymbol{\theta} - \boldsymbol{\nabla}\psi(\boldsymbol{\theta})$

$$\Rightarrow \Delta\beta_i = A_{ij}\Delta\theta_j + \frac{1}{2}D_{ijk}\Delta\theta_j\Delta\theta_k$$

$$\Rightarrow Q_{ijk}^{(s)} \approx \mathcal{A}_{il}\mathcal{A}_{jm}\mathcal{A}_{kn}Q_{lmn} + \frac{1}{2}(\mathcal{A}_{il}\mathcal{A}_{jm}\mathcal{D}_{kno} + \mathcal{A}_{jm}\mathcal{A}_{kn}\mathcal{D}_{ilo} + \mathcal{A}_{il}\mathcal{A}_{kn}\mathcal{D}_{jmo} - 4\mathcal{A}_{il}\mathcal{A}_{jm}\mathcal{A}_{kn}F_o)Q_{lmno}$$

$\Rightarrow$ Relation between source HOLICs and image HOLICs

Flexion

$$\Delta\beta_i = A_{ij}\Delta\theta_j + \frac{1}{2}D_{ijk}\Delta\theta_j\Delta\theta_k$$

$$A_{ij} = \delta_{ij} - \psi_{,ij} = \begin{pmatrix} 1-\kappa-\gamma_1 & -\gamma_2 \\ -\gamma_2 & 1-\kappa+\gamma_1 \end{pmatrix}$$

$$D_{ijk} = A_{ij,k} = -\psi_{,ijk}$$ Flexion

$$\mathcal{D}_{ijk} = \mathcal{F}_{ijk} + \mathcal{G}_{ijk}$$

$$\mathcal{F} = \mathcal{F}_1 + i\mathcal{F}_2 \equiv \partial\partial\partial^*\psi = |\mathcal{F}|e^{i\phi} = \partial\kappa$$ Spin-1 First Flexion

$$\mathcal{G} = \mathcal{G}_1 + i\mathcal{G}_2 \equiv \partial\partial\partial\psi = |\mathcal{G}|e^{3i\phi} = \partial\gamma$$ Spin-3 Second Flexion

Effects of Convergence, Shear, Flexion

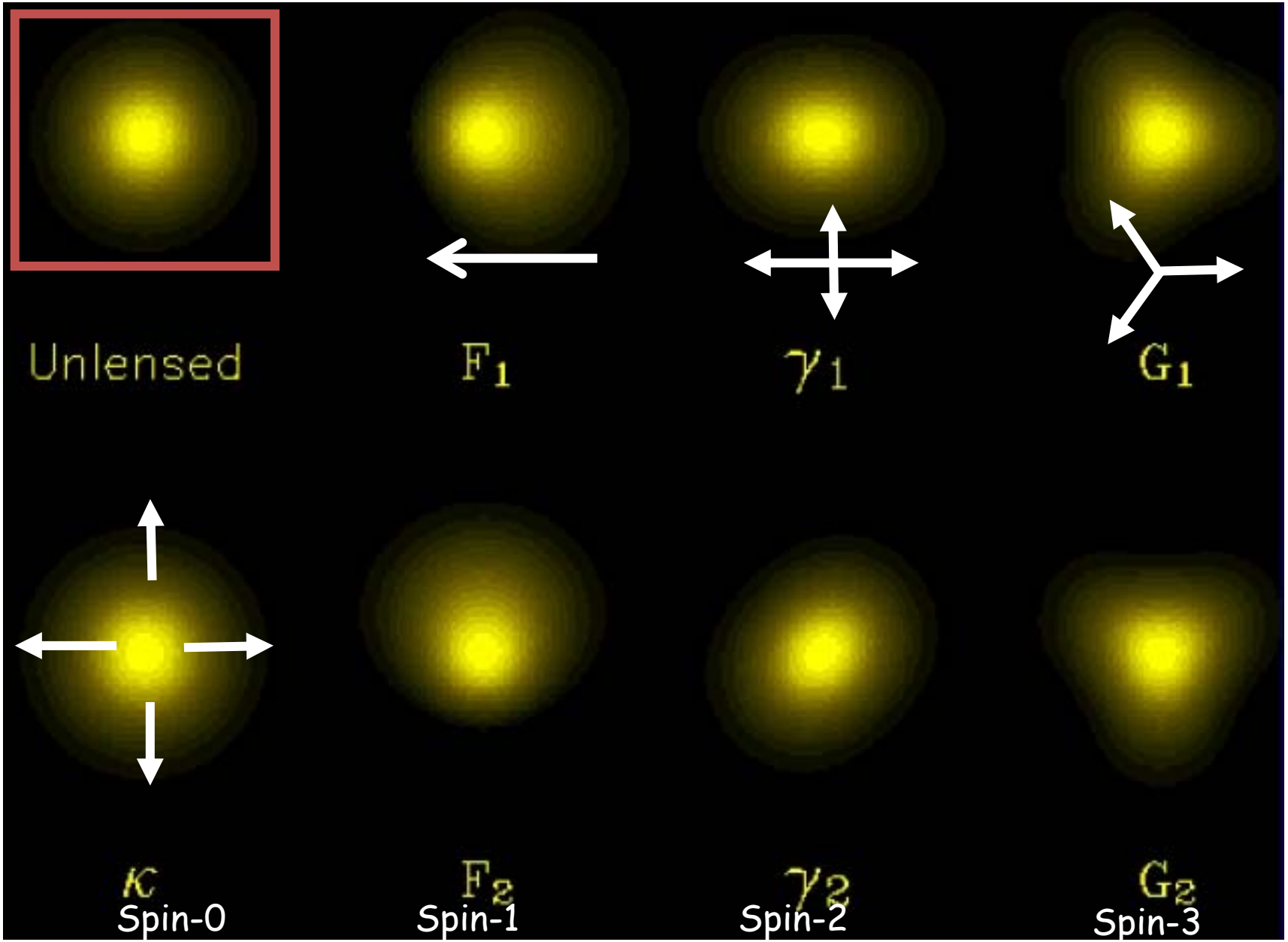

Where is Flexion useful?

An intermediate regime between WEAK and STRONG lensing can be well described by shearing and flexing effects:

Arclets = lensed images with slight curvatures

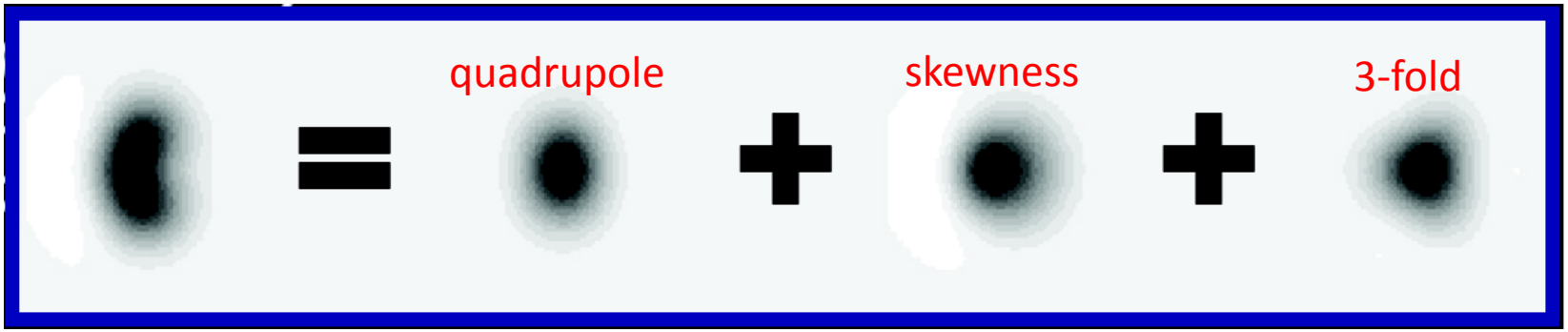

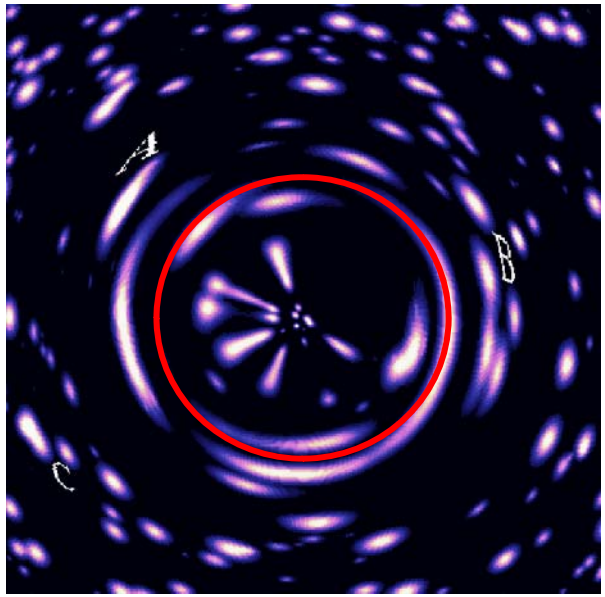

$$\gamma = \frac{1}{2}\partial\partial\phi \qquad F = \frac{1}{2}\partial^{*}\partial\partial\phi \qquad G = \frac{1}{2}\partial\partial\partial\phi$$

Spin-2 Spin-1 Spin-3

Goldberg & Natarajan 02, Bacon et al. 2005

Shear vs. Flexion

Resolution limit in ordinal (=Spin-2) weak lensing with ground based telescopes (Subaru, CFHT, etc.):

$$\mathrm{FWHM} = 0.'9 \left(\frac{\mathrm{S/N}}{5}\right) \left(\frac{\kappa}{0.2}\right)^{-1} \left(\frac{\sigma_\gamma}{0.4}\right)^{-1} \left(\frac{n_g}{30\mathrm{arcmin}^{-2}}\right)^{1/2}$$

Ordinal WL is sensitive to structures of 1'-10', which is dominated by clusters of galaxies

Flexion measures the gradient of shear; so is relatively sensitive to small-scale structures (e.g., groups of galaxies. Substructures in cluster)

$$\frac{S(F)}{S(\gamma)} \sim \frac{L\phi / r^3}{\phi / r^2} \sim \frac{L}{r}$$

L: image size

r: distance from the lens

Even though the higher-order effect is small, at small scales (r), for large images (L), Flexion signal might dominate over Shear signal

Relation between the source and image HOLICs

$$\zeta^{(s)} = \frac{\zeta - 2g\zeta^* - g^*\delta - \frac{1}{4}(8F^*\eta + 9F + 2G\eta^* + G^*\lambda)}{(1-\kappa)(1 - 4Re[g^*\lambda] - 5Re[F\iota_I^*] - Re[G\iota_{III}^*])},$$

$$\delta^{(s)} = \frac{\delta - 3g\zeta - \frac{1}{4}(10F\eta + 7F^*\lambda + 3G)}{(1-\kappa)(1 - 4Re[g^*\lambda] - 5Re[F\iota_I^*] - Re[G\iota_{III}^*])},$$

$$\zeta \equiv \frac{(Q_{111} + Q_{122}) + i(Q_{112} + Q_{222})}{\xi},$$

$$\delta \equiv \frac{(Q_{111} - 3Q_{122}) + i(3Q_{112} - Q_{222})}{\xi},$$

$$\xi \equiv Q_{1111} + 2Q_{1122} + Q_{2222}$$

$$\eta \equiv \frac{(Q_{1111} - Q_{2222}) + 2i(Q_{1112} + Q_{1222})}{\xi},$$ Spin-2

$$\lambda \equiv \frac{(Q_{1111} - 6Q_{1122} + Q_{2222}) + 4i(Q_{1112} - Q_{1222})}{\xi},$$ Spin-4

$$\iota_I \equiv \frac{(Q_{11111} + 2Q_{11122} + Q_{12222}) + i(Q_{11112} + 2Q_{11222} + Q_{22222})}{\xi},$$ Spin-1

$$\iota_{III} \equiv \frac{(Q_{11111} - 2Q_{11122} - 3Q_{12222}) + i(3Q_{11112} + 2Q_{11222} - Q_{22222})}{\xi},$$ Spin-3

$$\iota_V \equiv \frac{(Q_{11111} - 10Q_{11122} + 5Q_{12222}) + i(5Q_{11112} - 10Q_{11222} + Q_{22222})}{\xi},$$ Spin-5

In the weak lensing limit

$$\varsigma^{(s)} \approx \varsigma - \frac{9}{4} F$$

$$\delta^{(s)} \approx \delta - \frac{3}{4} G$$

Where F and G are the reduced Flexions

$$F := F_1 + iF_2 = \frac{\mathcal{F}}{1-\kappa}$$

$$G := G_1 + iG_2 = \frac{\mathcal{G}}{1-\kappa}.$$

Assuming $< \varsigma^{(s)} >=< \delta^{(s)} >= 0$

$$\langle \zeta \rangle \approx \frac{9}{4} \frac{\mathcal{F}}{1-\kappa} \approx \frac{9}{4} \mathcal{F},$$

$$\langle \delta \rangle \approx \frac{3}{4} \frac{\mathcal{G}}{1-\kappa} \approx \frac{3}{4} \mathcal{G}.$$

For the application to the actual observations

1. HOLICs should be evaluated with true center of the image

   The apparent center of the image is different from the true center that is mapped using the lens equation from the center of unlensed light.

2. We need a weight and PSF correction

$$Q_{ij\ldots k} \rightarrow Q^{obs}_{ij..k} \equiv \int d^2\theta\, I^{obs}(\theta)\Delta\theta_i\Delta\theta_j\cdots\Delta\theta_k\, W\left(\frac{|\Delta\theta|^2}{\sigma^2}\right)$$

Smearing effect by atomospheric turburence and imperfect optics is descibed by PSF(point spread function)

$$I^{obs}(\theta) = \int d^2\phi\, I(\phi)P(\theta-\phi)$$

The correction is made by using star images which are perfect point sources

Spin-1 PSF Anisotropy Correction: Application to Subaru A1689 data

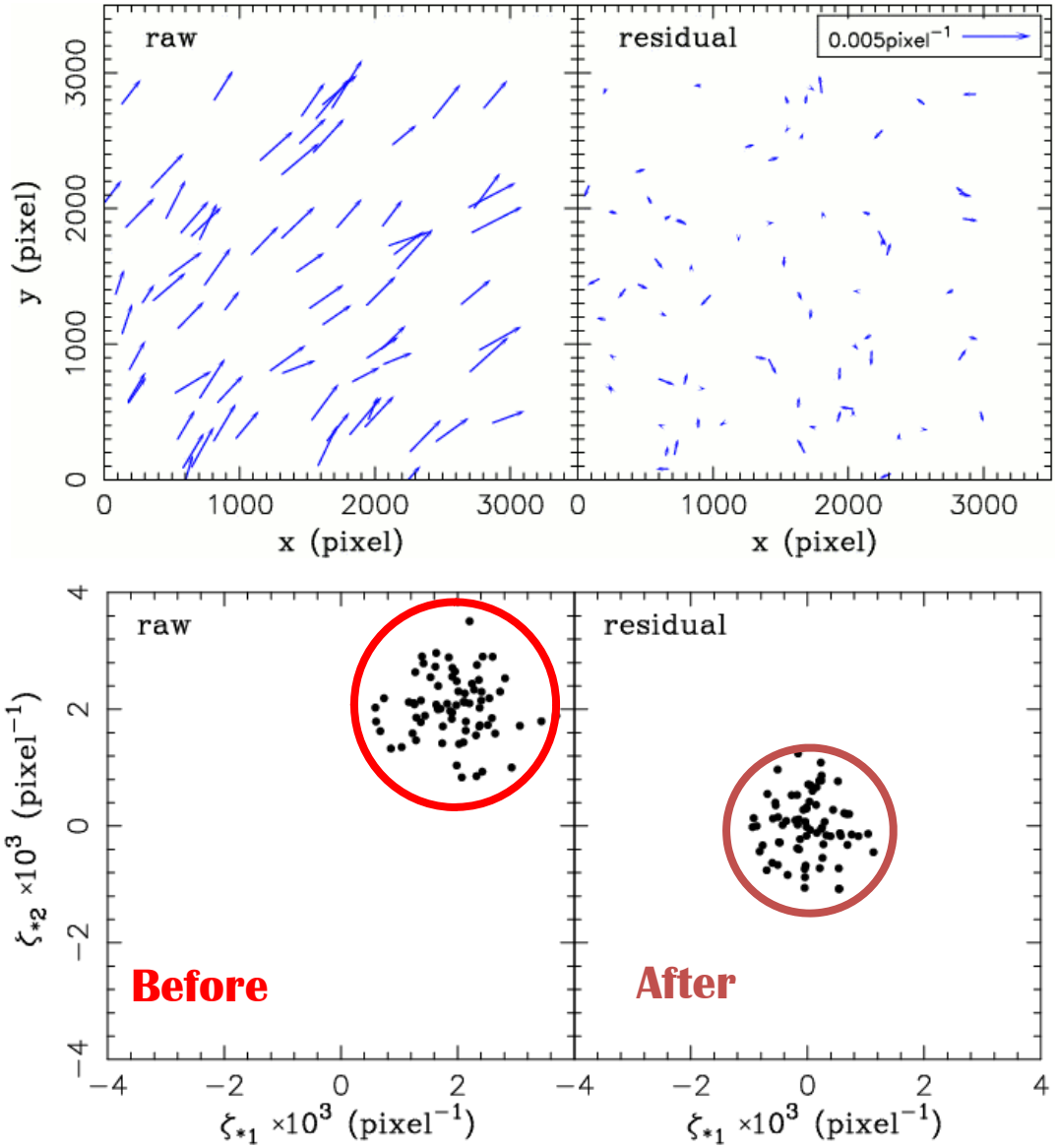

Spin-1 PSF anisotropy from stellar shape moments

$$\zeta_\alpha^{\,*} = (C^q)^*_{\alpha\beta}(\zeta_q^{\,*})_\beta$$

Okura, Umetsu, Futamase 2007b

Mass and Light in A1689 (Subaru)

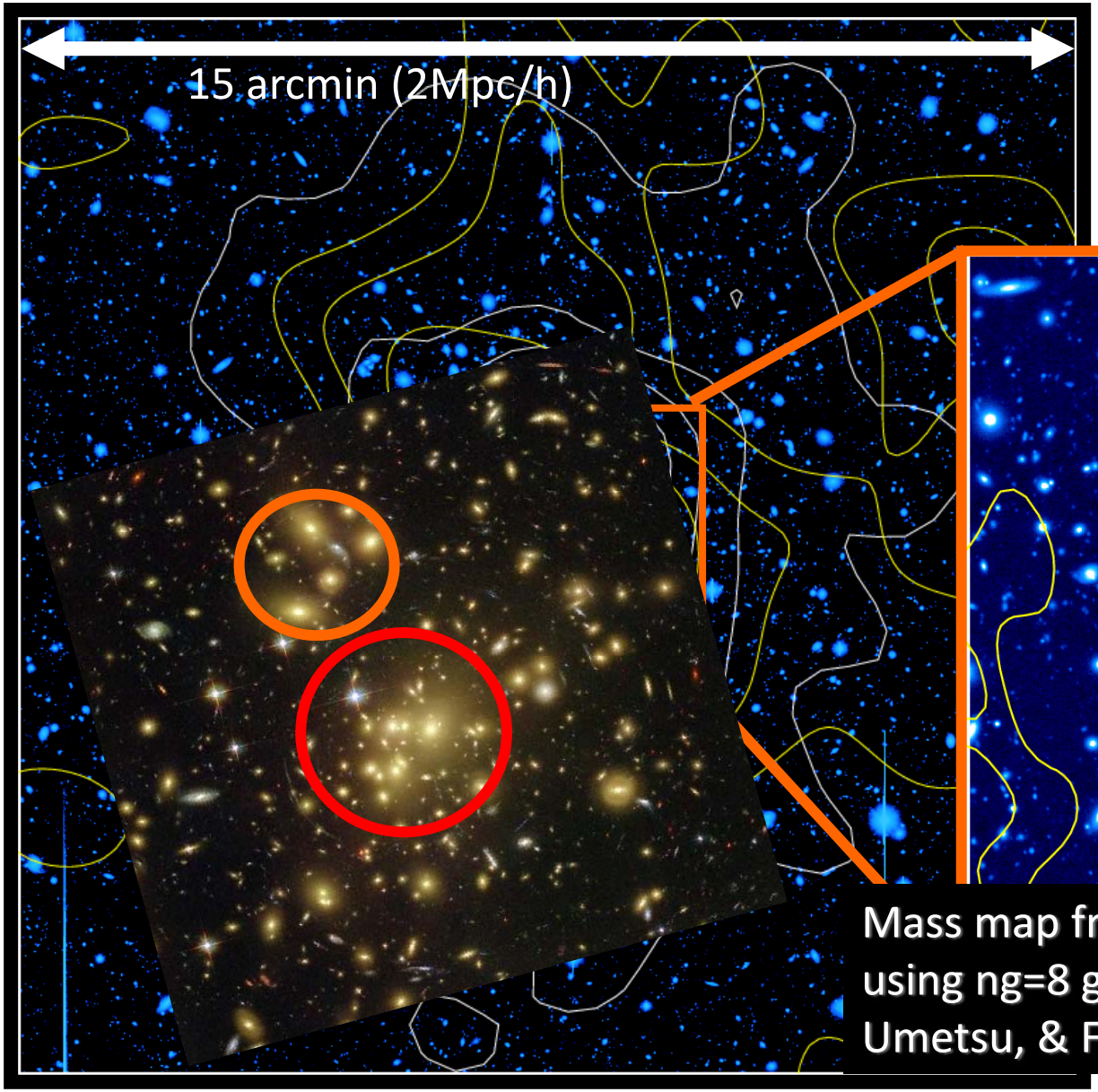

Mass + Light contours from Shear+Magbias data (Umetsu & Broadhurst

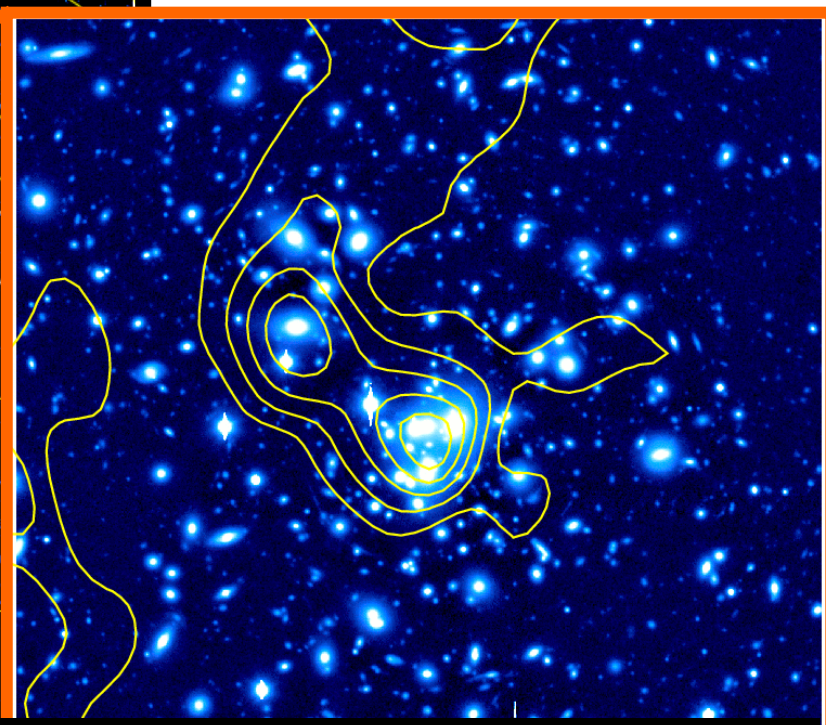

Mass map from Fleixon in a 4'x4' region using ng=8 gal/arcmin^2 !!! (Okura, Umetsu, & Futamase 2007b)

Mass Map of A1689 from Spin-1 Flexion

Mass reconstruction in the 4'x4' core region of A1689 (z=0.18)

E-mode (lensing)

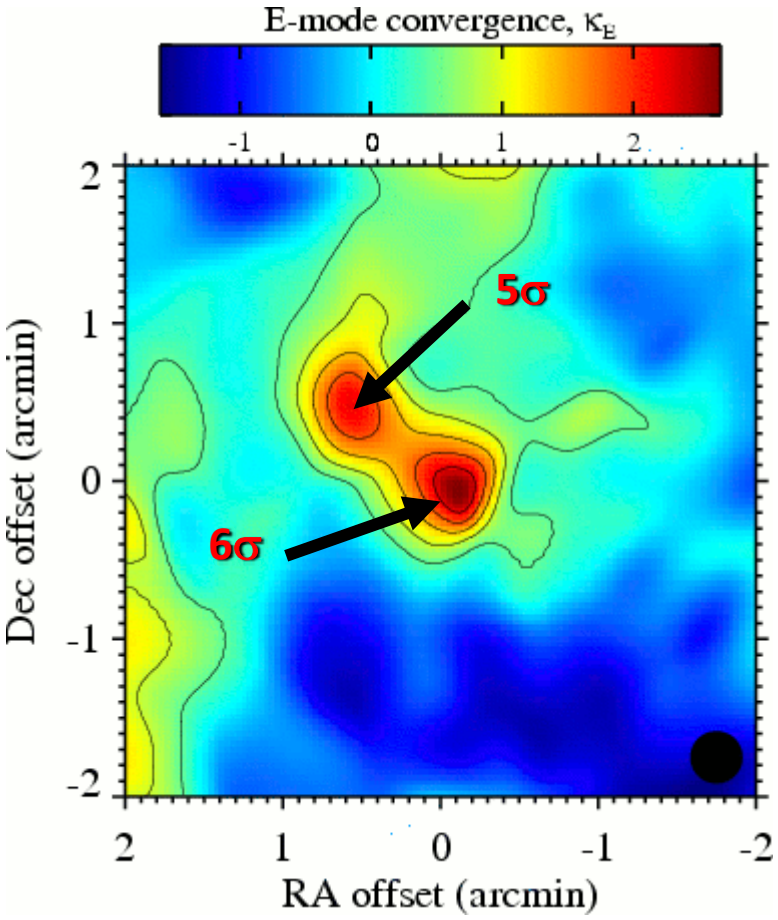

530kpc/h

B-mode (noise)

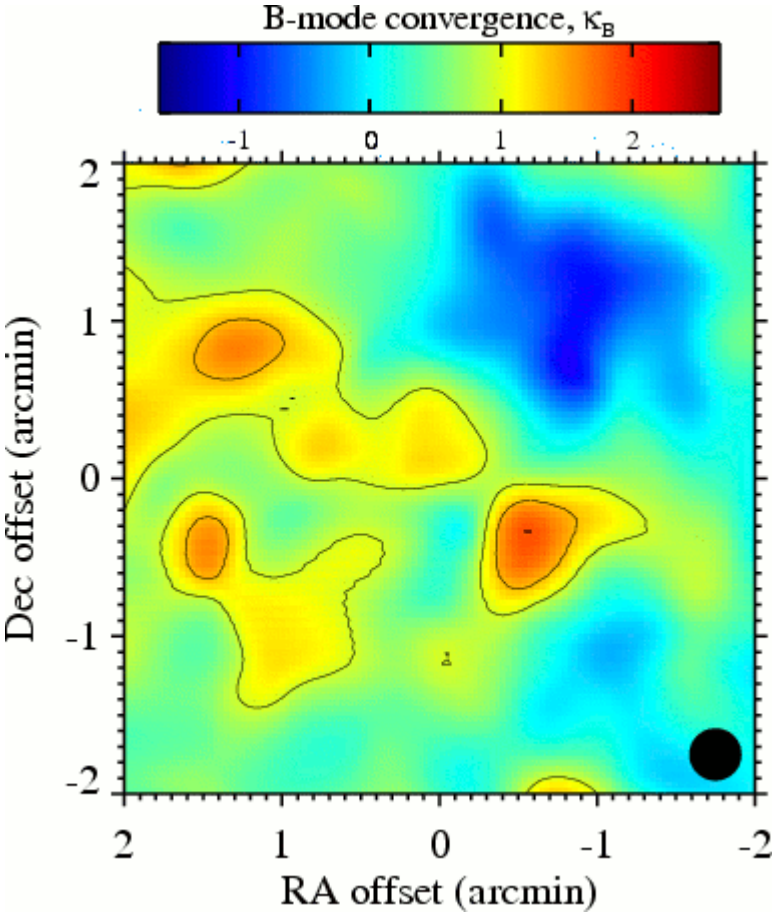

n_g=8 arcmin^-2

0.'3FWHM Gaussian

Okura, Umetsu, Futamase 2007b

Main Halo and sub halos

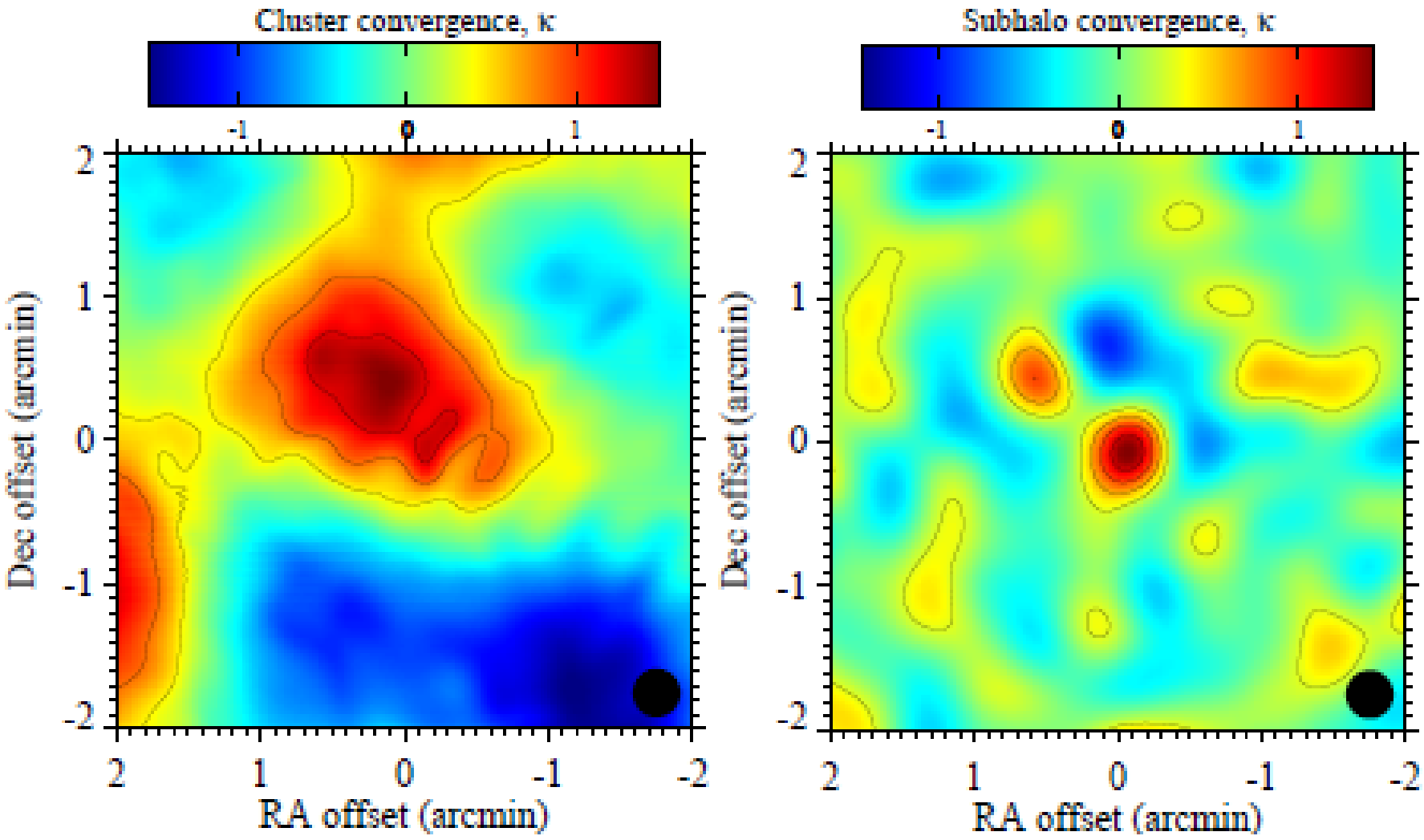

2: Spin-2 HOLICs

Our motivation

Is there any possibility to improve the accuracy of shear measurement using extra information in the existing data?

Shear is spin 2 quantity and is measured not only by ellipticity but also by spin-2 HOLICs of any order

Spin-2 HOLICs of different order will measure the shear in the different region of the image

There might be a possibility to improve the accuracy of shear measurement by averaging the measurement by spin-2 HOLICs up to some order

Definition of spin-2 HOLICs

Complex moments of image

$$Z_M^N \equiv \int d^2\theta X_M^N q[I(\boldsymbol{\theta})].$$

where X is the complex displacement in the image plane

$$\begin{aligned} X_1^1 &\equiv d\theta_1 + id\theta_2 \\ X_M^N &\equiv (d\theta_1 + id\theta_2)^{(N+M)/2}(d\theta_1 - id\theta_2)^{(N-M)/2} \end{aligned}$$

Then the Spin-2 HOLICs of order N is defined as follows

$$H_2^N \equiv \frac{Z_2^N}{Z_0^N}$$

In particular the usual complex ellipticity is N=2

$$\chi = H_2^2$$

Using the lens equation

$$Y_1^1 = (1-\kappa)(X_1^1 - g\ X_1^{1*}) \qquad g = \frac{\gamma}{1-\kappa}$$

We have a relation between the intrinsic spin-2 HOLICs and lensed spin-2 HOLICs

$$H^{(s)}{}_2^N \approx H_2^N - \frac{N+2}{2} g$$

Assuming that the expectation value of the intrinsic spin-2 HOLICs vanishes as usual

$$g = \left\langle \frac{2}{N+2} H_2^N \right\rangle$$

In practice we have to use the weighted HOLICs

$$Z_M^N \equiv \int d^2\theta I(\boldsymbol{\theta}) X_M^N W\left(\frac{X_0^2}{\sigma^2}\right)$$

Test by simulation (STEP)

difference

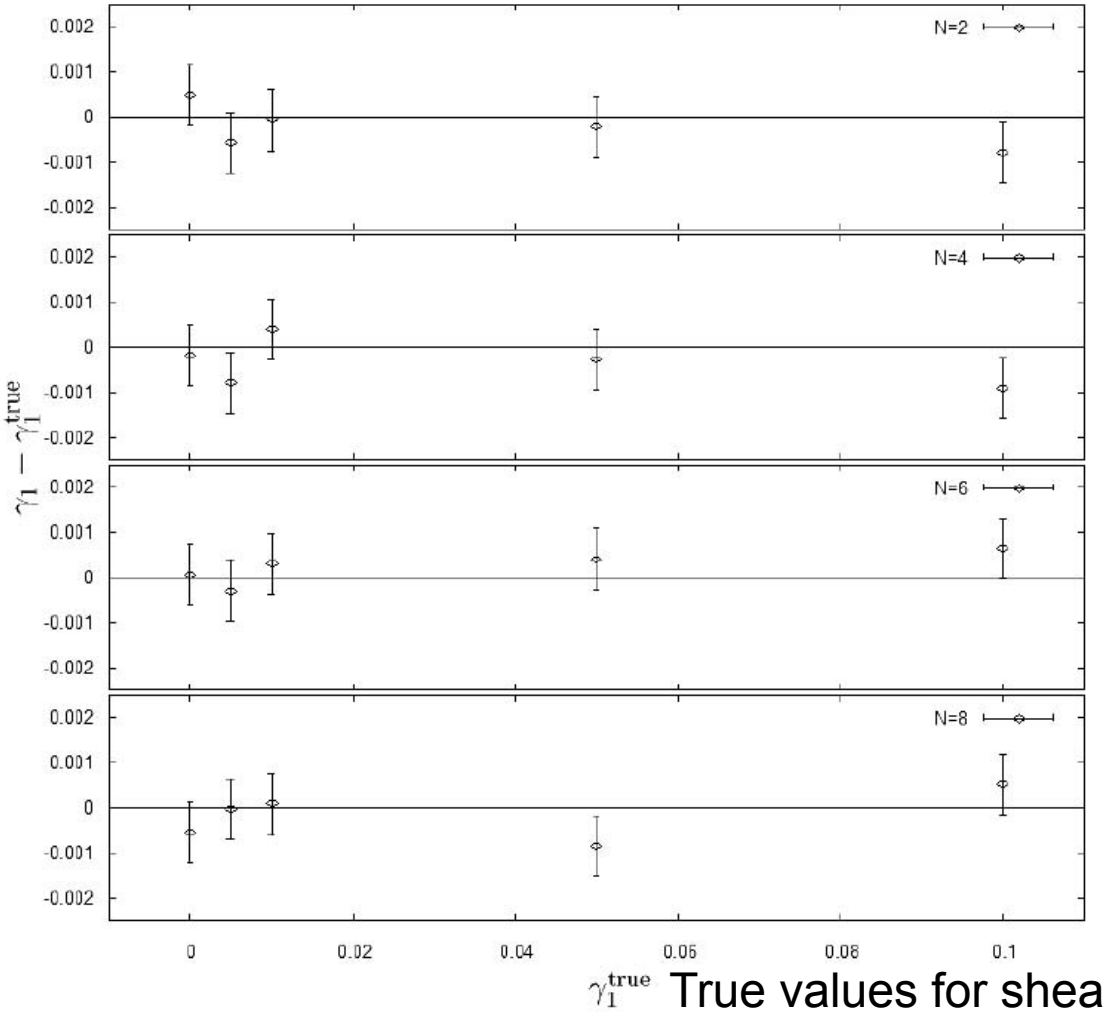

Fig. 1.— The results of analysis of STEP1 simulations in each order of HOLICs shear measurement. The horizontal axis are the true(input) shear, and the vertical axis are the difference of estimated and true shear with 1σ errors. Errors of estimated shear are same levels and less than 1σ error in All order.

Application to A1689

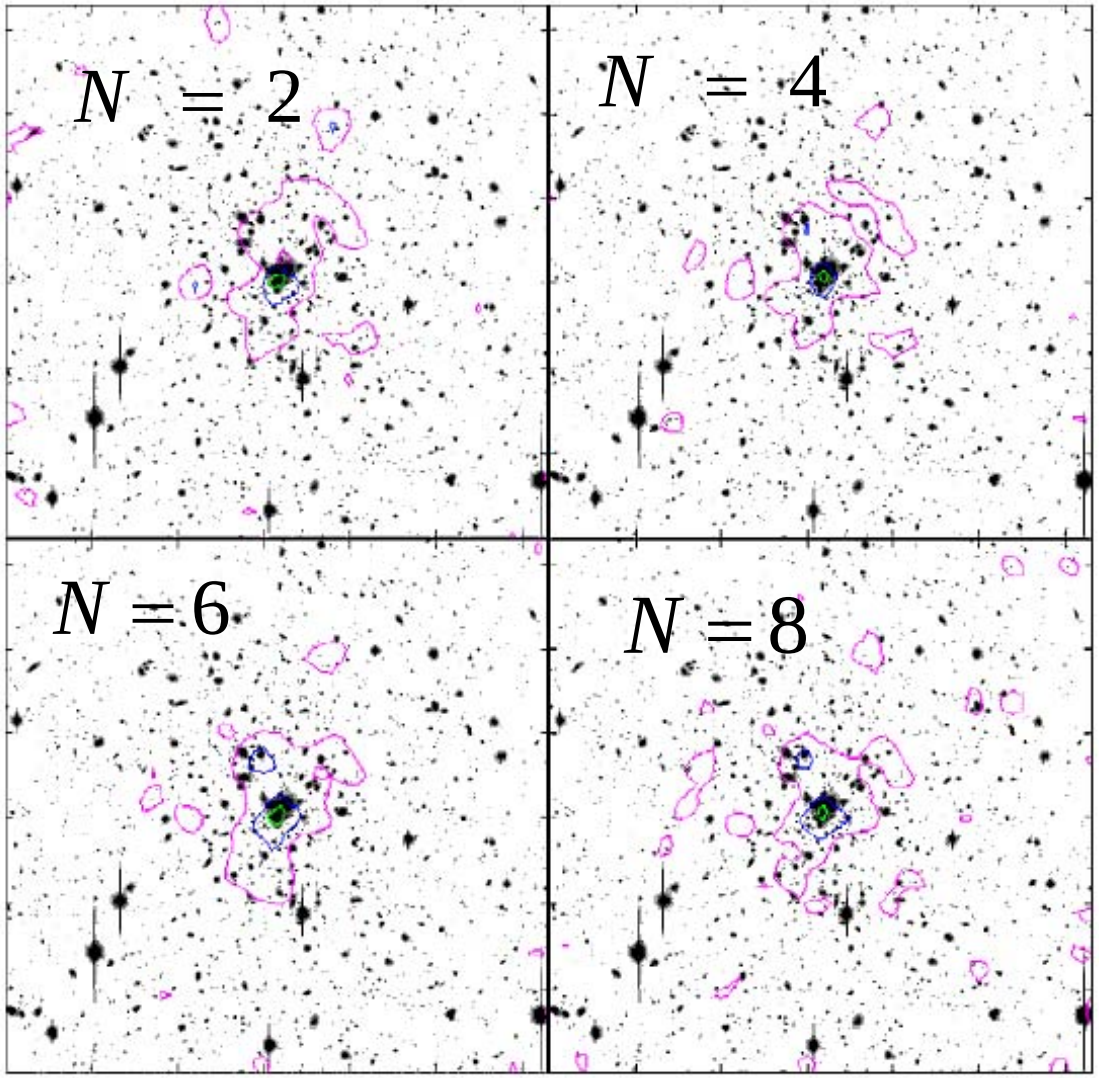

Fig. 1.— The reconstructed mass distribution in the central $10' \times 10'$ region of A1689 by spin-2 HOLICs of various order up to 8. The contours are spaced in units of $1\sigma(\approx 0.2)$ North is to the top, and East to the left.

Subaru S-Cam i'-band data

3366 galaxies(about 33 /arcmin) with 2.5<rh<10 and 22<MAG<25.5 are used in the mass reconstruction

The smoothing is 0.15" by Gaussian radius the interval of contours is ⊿κ=0.2, the lowest Contour is κ=0.2

Reconstructed B-mode dispersion 1σ=0.065,0.060, 0.062, 0.073 for N=2,4,6, 8, respectively

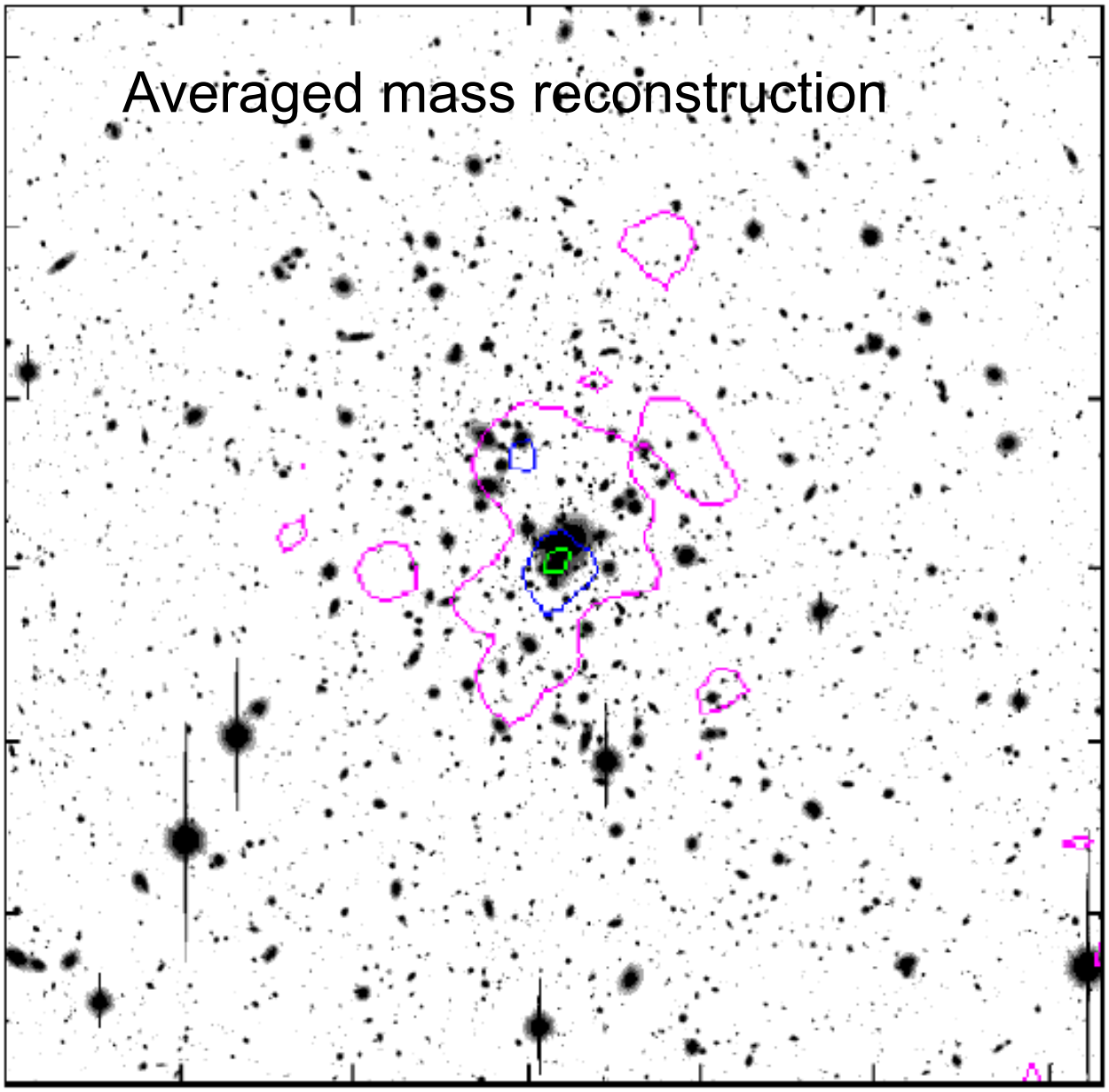

Fig. 2.— The averaged mass distribution in the same region of Fig.1 over that measured by spin-2 HOLICs of order N up to 8.

Averaged B-modes has dispersion $1\sigma \sim 0.059$

Future

- More observation for clusters to observationally establish c-M relation and compare with theory
- Accurate determination of mass structure using Strong and weak lensing for many clusters with appropriate redshifts to constrain the dark energy properties
- Improvement of PSF correction for HOLICs to have more accurate mass estimation to reveal substructures of clusters
- Application of spin-2 HOLICs to cosmic shear
- Lensing effects on CMB and 21 cm

There will be many applications of weak lensing to observational cosmology with new instruments such as Hyper S-Cam , ALMA and planned 21 cm telescopes